U.S. DEPARTMENT OF THE INTERIOR

GEOLOGICAL SURVEY

The Electrical Properties of Clay

by

W. R. Sill and J. D. Klein

Department of Geology and Geophysics

University of Utah, Salt Lake City, Utah

Open-File Report 81-989

1981

The Electrical Properties of Clay

Final Report

For the period February 1, 1980 through January 31, 1981

Work performed under contract no. 14-08-0001-18718

Department of Geology and Geophysics, University of Utah

W. R. Sill and J. D. Klein

February 1981

The Electrical Properties of Clay

by

W. R. Sill and J. D. Klein

INTRODUCTION

The effects of clay on the frequency-dependent electrical impedance of rocks has not been investigated with the same intensity as have the effects of conductive minerals, such as sulfides. Investigators in the mining geophysical community who have examined clay effects have been primarily concerned with polarization phenomena. Most notable is the work of Vacquier et al (1957) and Madden and Marshall (1959) who describe, respectively, time-domain IP measurements on artifical clay-sand mixtures and a theoretical model for membrane (clay) polarization. Olgilvy and Kuzmina (1972) described additional time-domain measurements on artifical mixtures, while Roy and Elliott (1980) used horizontal layers of varying clay-sand composition to model negative apparent chargeabilities due to geometric effects. The theoretical model of Madden and Marshall (1959) was simplified and compared to measurements made on natural samples of dirty sandstone by Sill (1964). It is generally accepted that membrane polarization is a result of differences in mobility between anions and cations in adjacent zones in pore passages. Polarization is then due to concentration gradients that develop at zone boundaries in response to current flow. This implies that electrical properties differ from place-to-place within the rock, and that the clay distribution is not uniform when examined on a fine enough scale.

The dependence of resistivity on clay type and content has been examined in some detail by individuals interested in predicting porosity and hydrocarbon saturation from well logs of resistivity. Waxman and Smits (1972) and Waxman and Thomas (1976) present a semi-empirical model for describing the dependence of resistivity on clay content, expressed as cation exchange capacity (CEC) per unit pore volume. They assume that resistivity is frequency independent and that all of the clay in their samples contributed to the observed decrease in resistivity. This implies that the clay is uniformly distributed throughout the rock and that paths of conduction along clay surfaces are continuous. It is unclear how the Waxman-Smits model would apply for estimating the CEC per unit pore volume for polarizable samples. Unfortunately there does not exist presently a sufficiently quantitative model for predicting clay content for such polarizable material.

It is evident that a systematic and thorough laboratory study is needed in order to completely understand the effects of clay. A more complete data base is needed in order to test various rock models. To this end we have undertaken a laboratory investigation of the electrical properties of natural clay-bearing rocks and mixtures of clay and glass beads. Our main objective was to measure the spectral characteristics of these materials, and to compare results to various rock models. A secondary objective was to compare the nonlinear response of clay-bearing materials to observations presented by Olhoeft (1977a, 1977b, 1978, 1979) and Olhoeft and Scott (1980), who have observed unusual nonlinear properties for various ion exchange materials.

LINEAR IMPEDANCE

The Madden-Marshall Model

Madden and Marshall (1959) present a theoretical model for membrane polarization. They assume that the membrane is composed of a series combination of zones with equal area but unequal transference number. It is assumed that zone 1 contains pore fluid which is uninfluenced by clay and therefore has normal electrical properties. The pore fluid in zone 2 is supposed to be in near proximity to clay particles. The exchange cations associated with the clay have a tendency to dissociate into the solution, imparting an increase in concentration of cations near the clay particle. Some of the anions, however, are permanently bound to the clay mineral lattice. Thus, when current is passed through the zone, it is carried predominantly by transport of cations rather than anions. Madden and Marshall treat this enhanced conduction by cations simply as a difference in transference number between anions and cations, thus lumping together the concentration and mobility for each type of ion. Thus, their model loses any precise quantitative relationship with the excess surface charge associated with the clay, which is related to the CEC per unit pore volume of the Waxman-Smits model. Although the Madden-Marshall model may present an adequate physical description, it is not amenable for use as a quantitative rock model. It is worth further consideration here, however, since it can provide some insight into the dependence of clay response on various model parameters which are physically meaningful.

After linearizing the appropriate equations of motion and matching boundary conditions between zones, Madden and Marshall derive a rather complicated expression for the impedance of a series combination of zones.

$$z(w) = \frac{L_1}{\mu_1 P_o F}\left\{\frac{1}{\sigma_1\theta_1} + \frac{B}{A\sigma_2\theta_2} + \frac{(\sigma_2 - \sigma_1)^2}{\sigma_2^2\sigma_1^2\theta_2\theta_1\left[\frac{X_1\theta_2}{\tanh X_1} + \frac{X_2\theta_1 A}{B\tanh X_2}\right]}\right\} \qquad (1)$$

where

μ_1 = ionic mobility in zone 1,

F = Faraday constant,

P_o = bulk concentration of cations,

D = diffusivity,

t = transference number,

ω = angular frequency,

1 = index for zone 1,

2 = index for zone 2,

L = zone length,

$A = L_1/L_2$,

$B = D_1/D_2$,

$\sigma = t^-/t^t$,

$$X_i = \frac{r_1 L_1}{2},$$

$$\theta_i = \frac{\sigma_i + 1}{\sigma_i},$$

$$r_1 = \left(\frac{j\omega\theta_i}{2D_i}\right)^{1/2}.$$

At low frequency $Z(\omega)$ can be approximated by a parallel RC circuit. This

behavior can be understood by considering a completely anionic selective zone in which cations move unhindered and for which anions are completely blocked at zone boundaries. The build-up of charge at the boundaries gives rise to the capacitive behavior. At high frequency, tanhx→1, and $Z(\omega)$ take the form of a series combination of a resistance and a Warburg impedance. The presence of a Warburg impedance implies that diffusion of ions to and from the zone boundaries is an important process. For both $\omega \to 0$ and $\omega \to \infty$, $Z(\omega)$ becomes purely resistive,

$$Z(o) = \frac{L_1}{\mu_1 P_o F}\left\{\frac{1}{\sigma_1\theta_1} + \frac{B}{A\sigma_2\theta_2} + \frac{(\sigma_2 - \sigma_1)^2}{\sigma_2^2\sigma_1^2\theta_1\theta_2(\theta_2 + \frac{\theta_1 A}{B})}\right\}$$

$$Z(\infty) = \frac{L_1}{\mu_1 P_o F}\left\{\frac{1}{\sigma_1\theta_1} + \frac{B}{A\sigma_2\theta_2}\right\}$$

Figures 1 through 3 display amplitude and phase of $Z(\omega)$ as a function of frequency for the indicated model parameters. The amplitudes have been normalized to a dc value of 1.0. Note that the phase, plotted on a logarithmic scale, varies with a slope of 1 and -1/2 at low and high frequency, respectively. This corresponds to the capacitive and diffusive behavior discussed previously. Figure 1 shows the effect of variation in L_1, the distance between selective zones. As L_1 increases, the relaxation shifts to lower frequency, but otherwise remains unchanged. The amount of the shift is equal to $(L_1)^2$. Figures 2 and 3 display the results of varying A and σ_2. In each case, the frequency effect shows a strong dependence, with only a slight

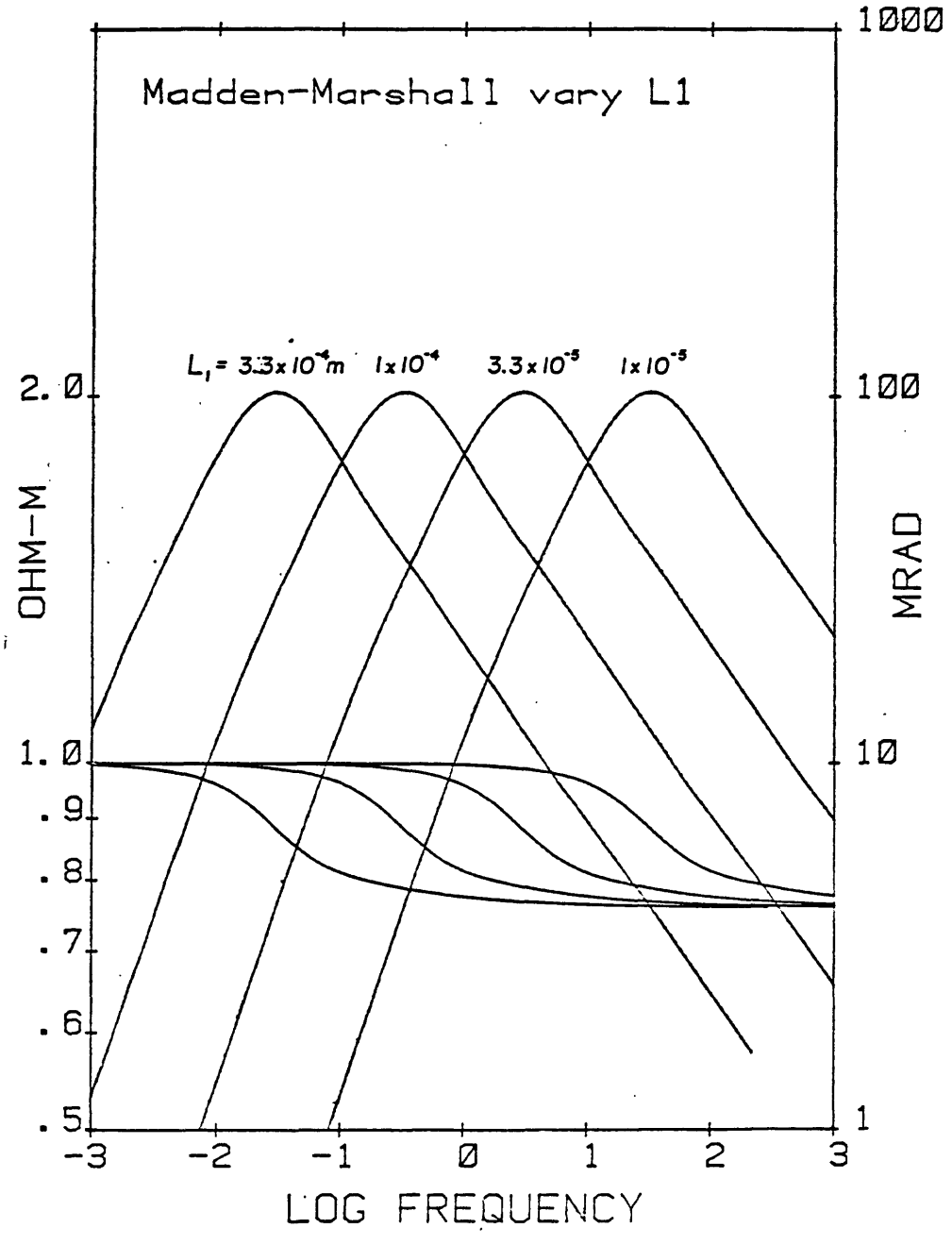

Figure 1.--Dependence of the Madden-Marshall model on L_1. Normalized amplitude and phase calculated for A = 1, B = 1, σ_1 = 1, D_1 = 2 x $10^{-9}m^2$/sec, σ_2 = 0.01.

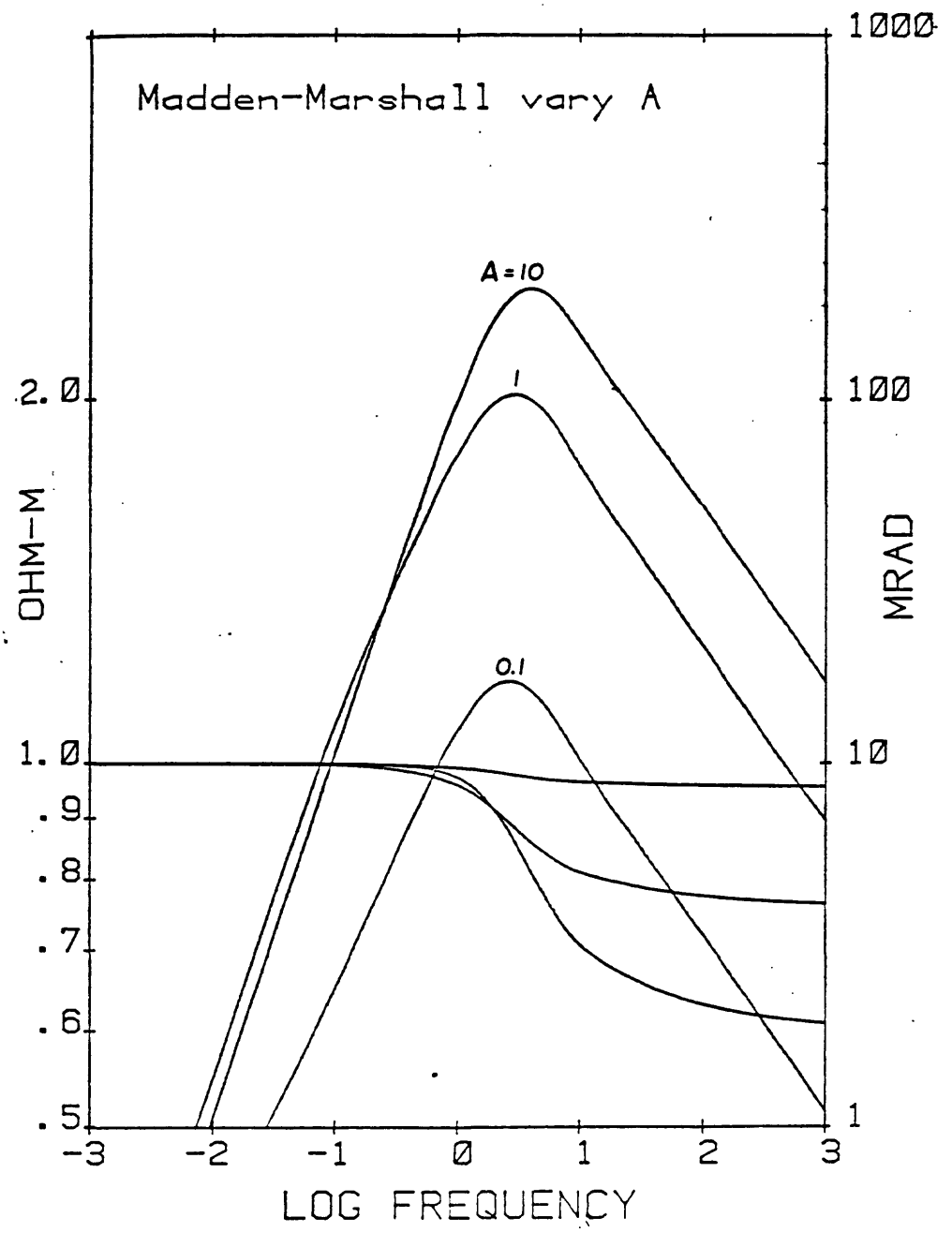

Figure 2.--Dependence of the Madden-Marshall model on A. Normalized amplitude and phase calculated for $L_1 = 3.3 \times 10^{-5}$m, B = 1, $\sigma_1 = 1$, $D_1 = 2 \times 10^{-9}$m^2/sec, $\sigma_2 = 0.01$.

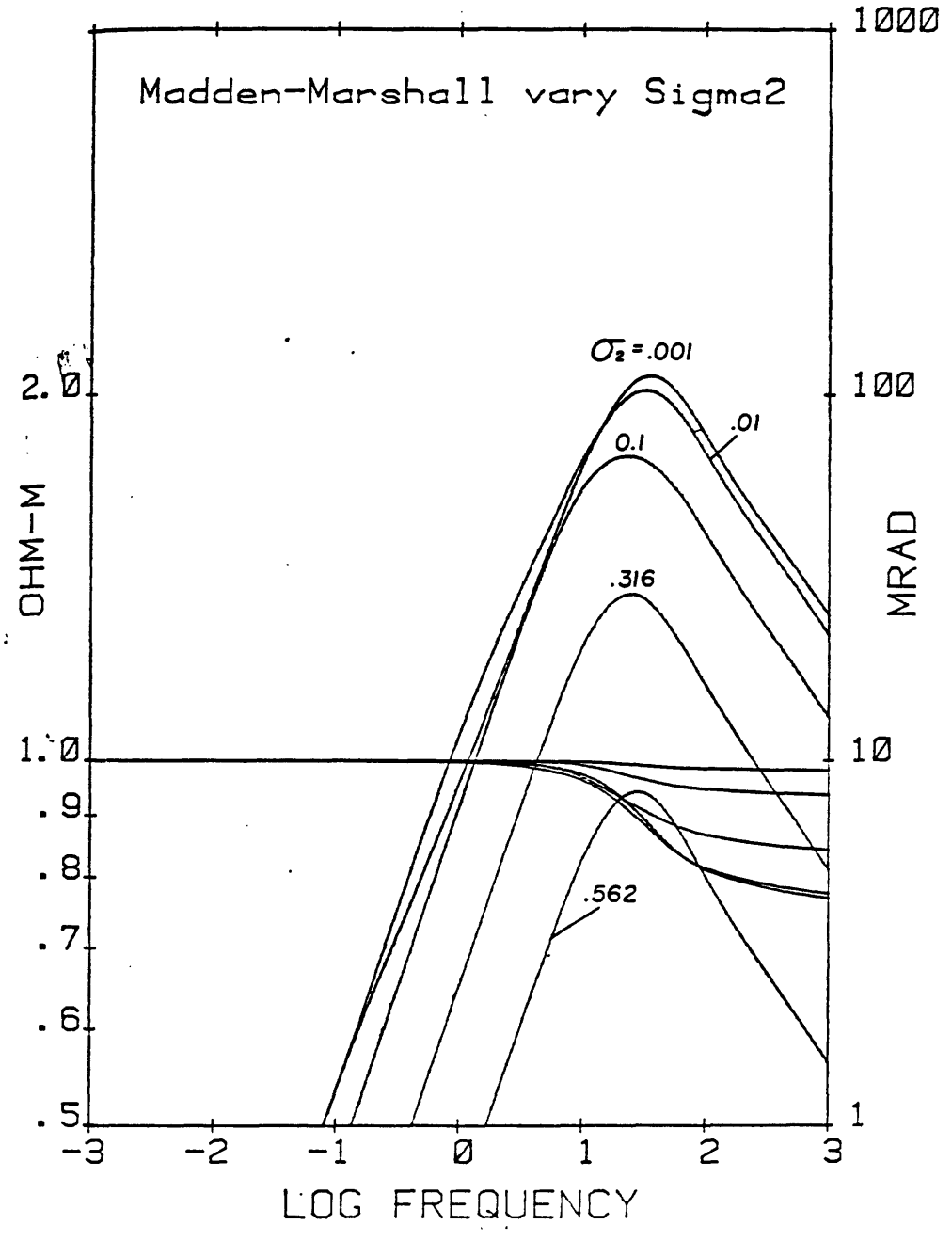

Figure 3.--Dependence of the Madden-Marshall model on σ_2. Normalized amplitude and phase calculated for $L_1 = 1 \times 10^{-5}$m, A = 1, B = 1, $\sigma_1 = 1$, $D_1 = 2 \times 10^{-9}$m^2/sec.

change in the frequency of the relaxation. Increased A corresponds to a decrease in length of the selective zone, for L_1 fixed. An increase in A also corresponds to a decrease in the volume fraction of pore space which is selective. This model then leads to the puzzling prediction that decreased clay content will lead to an increased frequency effect which is at odds with observations for small clay concentrations. Decreased σ_2 leads to an increased frequency effect, as would be expected for an increase in selectiveness of the clay zones. This would sensibly predict that clay with increased CEC would produce larger frequency effects. Because of the high negative correlation between A and σ_2, the Madden-Marshall model is, in general, inadequate for quantitative predictions of clay content or CEC. If detailed information were available on the occurrence and texture of clay particles in a rock, then it might be possible to place constraints on the value of A. The frequency effect could then be used to obtain estimates of σ_2. Alternately, if σ_2 could be constrained, then it might be possible to make some estimate of the quantity of clay present.

The form of the plots in figures 1 through 3 suggests that $Z(\omega)$ can be approximated by a Cole-Davidson distribution (Pelton, 1977):

$$Z_{cd}(\omega) = R_o \left(1 - m \left(1 - \frac{1}{(1 + j\omega\tau)^a}\right)\right) \qquad (2)$$

where

a = 1/2,

R_o = background resistivity,

$m = 1 - \frac{R_\infty}{R_o}$ = chargeability,

τ = time constant,

R_∞ = high frequency aysmptote.

It is not possible to cast $Z(\omega)$ (equation (1)) exactly in the form of a Cole-Davidson distribution. To compare $Z(\omega)$ and $Z_{cd}(\omega)$ (equation (2)) theoretical values of amplitude and phase from figure 1 for $L_1 = 3.3 \times 10^{-5}$m were inverted simultaneously to equation (2), with results shown in figure 4. The Cole-Davidson distribution does provide a close fit to the Madden-Marshall model. Because of the reduced number of parameters, the Cole-Davidson distribution may constitute a more practical tool for characterizing clay response. From the Madden-Marshall model, we could predict that the time constant τ would depend primarily on the distance between clay zones. Thus, τ could provide information on the clay occurrence and texture. The chargeability, m, would be expected to depend on both the amount of clay present in isolated zones and the CEC. Clay which provided a continuous path for surface conduction, as assumed in the Waxman-Smits model, would be expected to decrease R_o, but have no effect on m.

The above discussion suggests that the Cole-Davidson distribution may be appropriate for empirically describing membrane polarization. In the following section, we present data which were obtained with artifical clay-glass bead mixtures and which have been inverted and interpreted in terms of a generalized Cole-Davidson distribution.

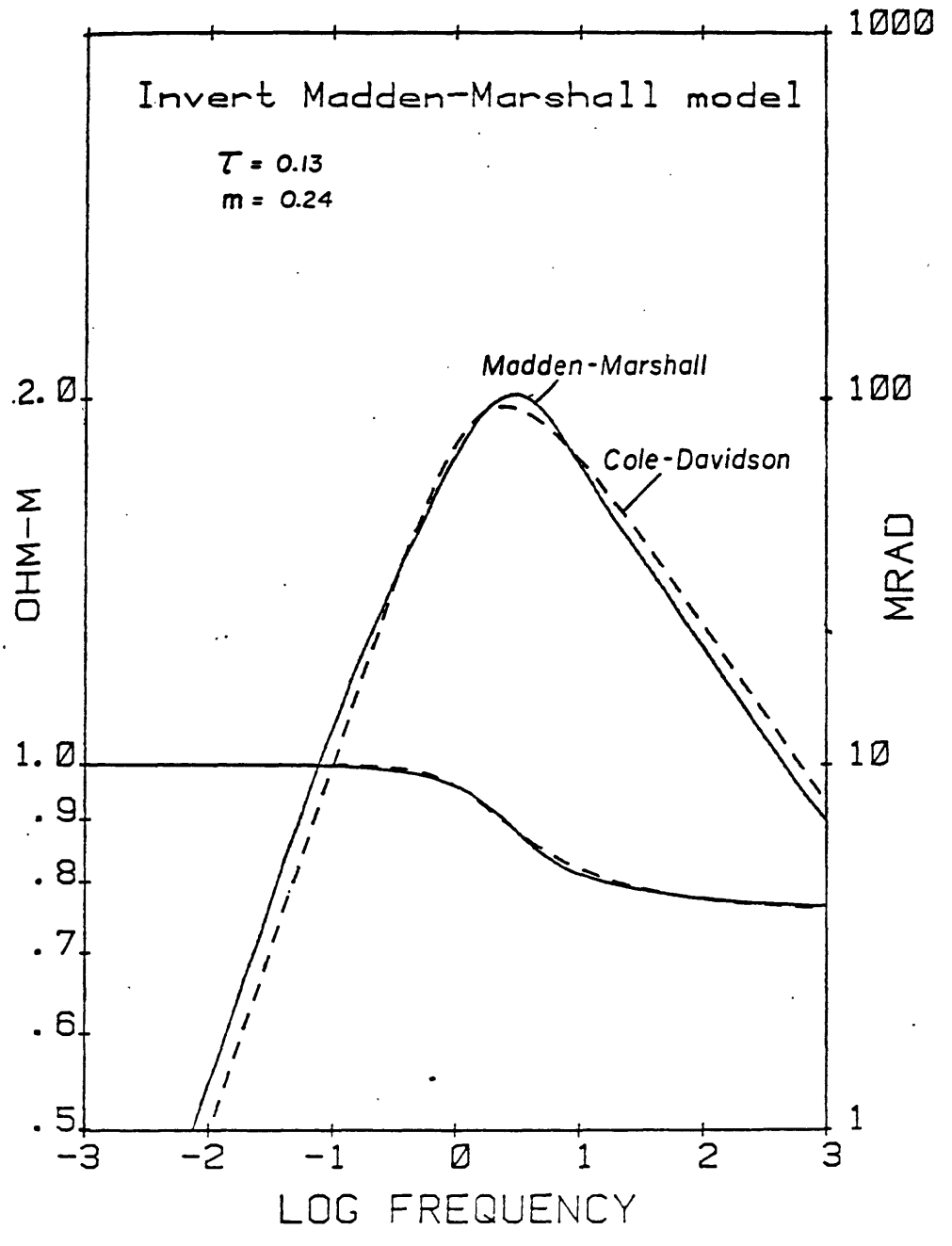

Figure 4.--Results of inverting theoretical data from the Madden-Marshall model to the Cole-Davidson distribution.

Measurements on Artificial Mixtures

A number of measurements were made on kaolinite and montmorillonite mixed with glass beads of varying size. In addition, the conductivity of the pore solution was varied with the addition of NaCl. Measurements of amplitude and phase were made mostly over the range of 1/128 to 1024 Hz using a ZONGE receiver. The usual procedure was to mix wet the desired quantity of clay with glass beads. The mixture was then packed into sections of plexiglass tubing after which fine nylon screen was fastened on the ends. The samples were allowed to dry and were then vacuum-saturated with the desired solution. A high humidity cell (fig. 5) was used to mount the samples such that 4-electrode measurements could be made.

Figures 6 through 9 display typical observed spectra for artificial samples. The amplitude and phase have been inverted simultaneously to a generalized Cole-Davidson distribution (Pelton, 1977):

$$Z^1(\omega) = R_i\left(1 - m\left(1 - \frac{1}{(1 + (j\omega\tau)^c)^a}\right)\right).$$

For this model, the phase has slopes of c and -ac at low and high frequency, respectively, on a plot of log (ϕ) versus log (ω). The solid lines in figures 6 through 9 give the theoretical results for the best fit model in each case. The asymmetric phase peaks and steep phase slopes at low frequency provide support for the Madden-Marshall model as correctly describing membrane polarization. If membrane polarization could be completely characterized by diffusion-like processes instead, then we would expect more symmetric phase peaks with the parameter, a, close to 1.0. Figure 10 represents histograms of

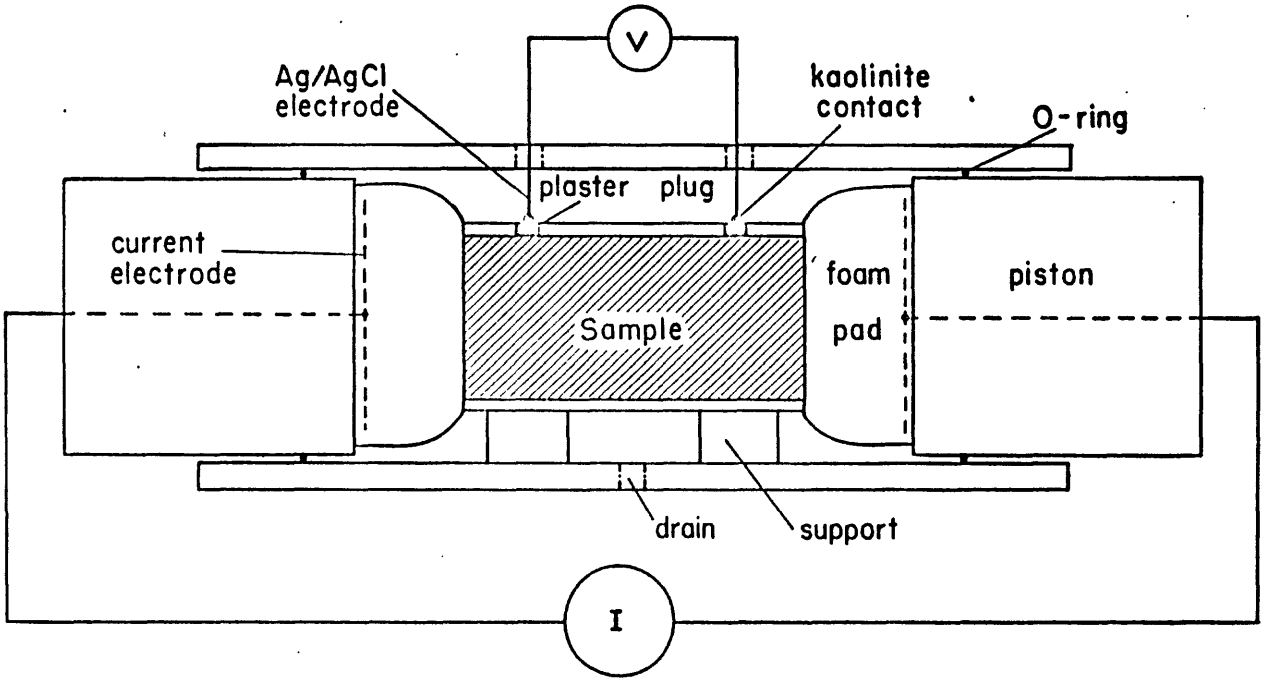

Figure 5.--Schematic of high humidity electrode cell used in impedance measurements on artificial and natural samples.

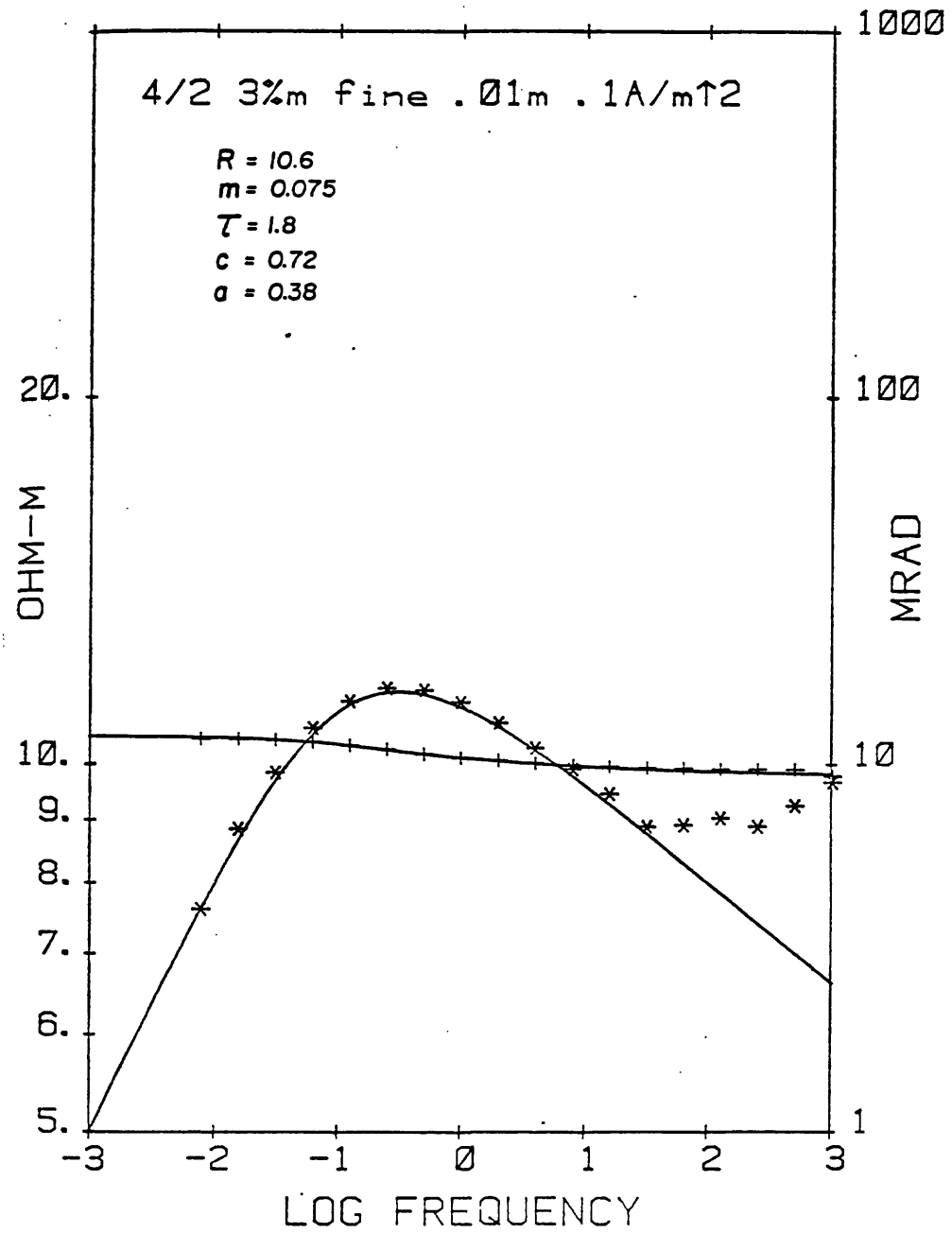

Figure 6.--Observed amplitude and phase and inversion results for 3 percent Ca-montmorillonite by weight, fine glass beads, 0.01m NaCl, 0.1 A/m^2.

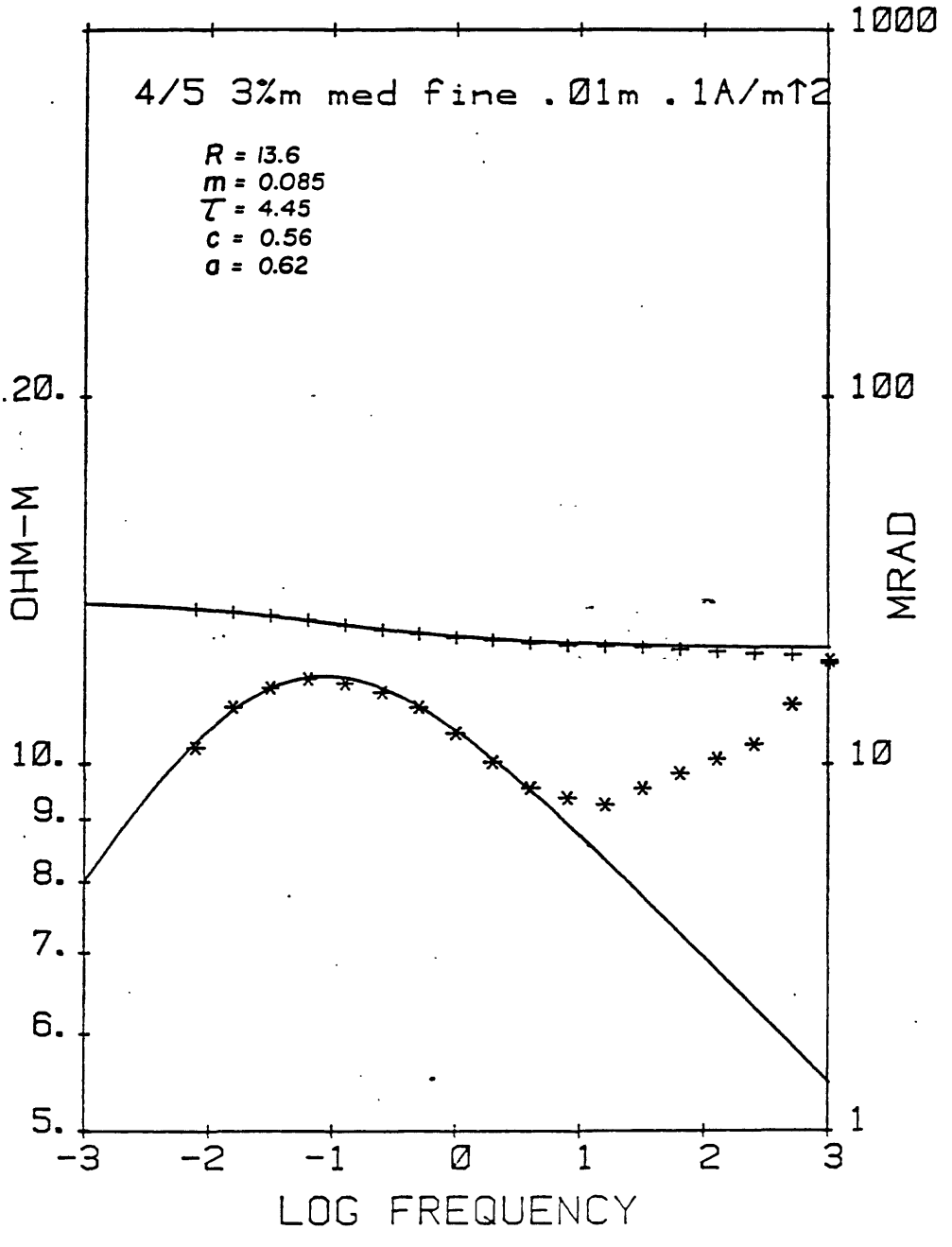

Figure 7.--Observed amplitude and phase and inversion results for 3 percent Ca-montmorillonite by weight, medium-fine glass beads, 0.01m NaCl, 0.1 A/m^2.

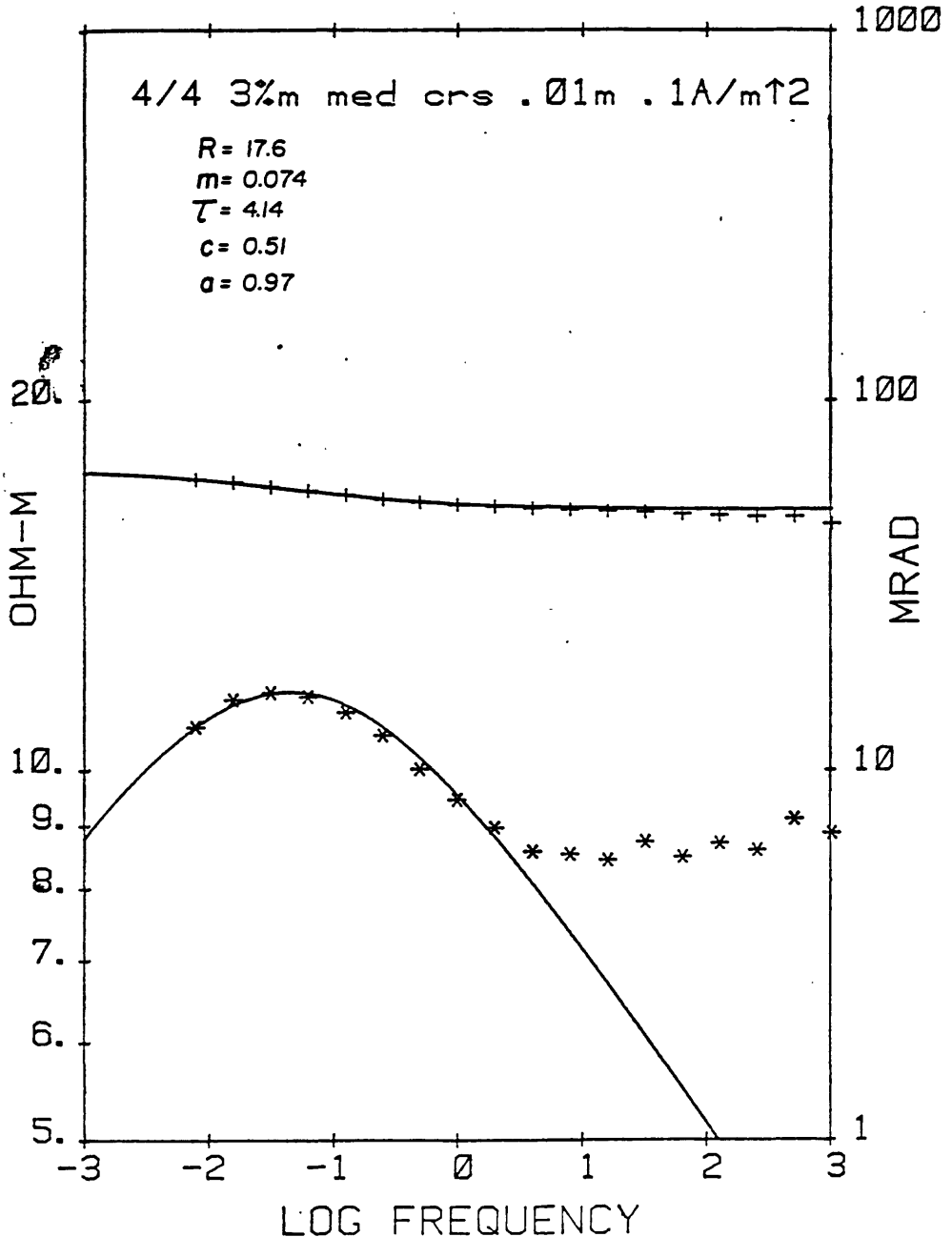

Figure 8.--Observed amplitude and phase and inversion results for 3 percent Ca-montmorillonite by weight, medium-coarse glass beads, 0.01m NaCl, 0.1 A/m^2.

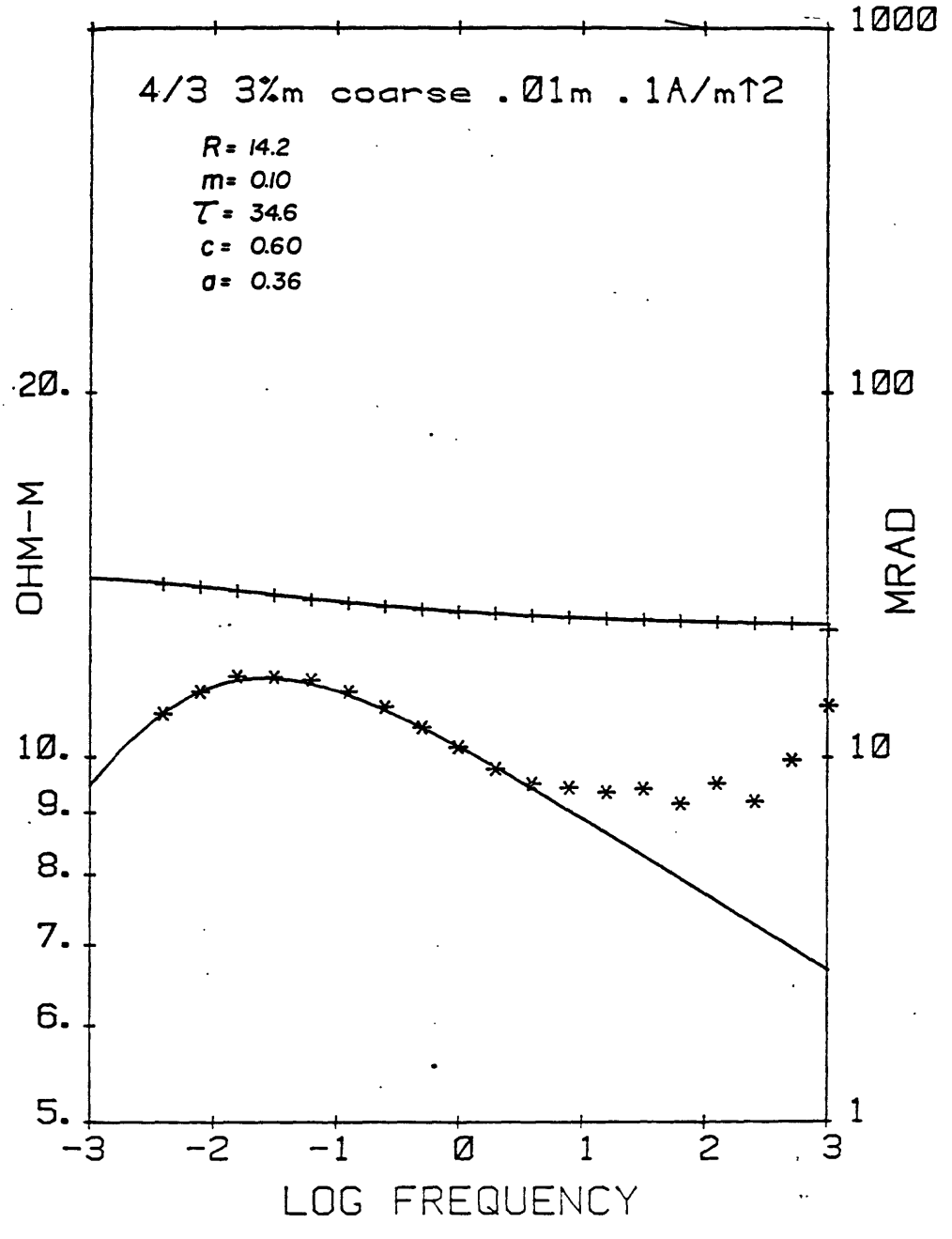

Figure 9.--Observed amplitude and phase and inversion results for 3 percent Ca-montmorillonite by weight, coarse glass beads, 0.01m NaCl, 0.1 A/m^2.

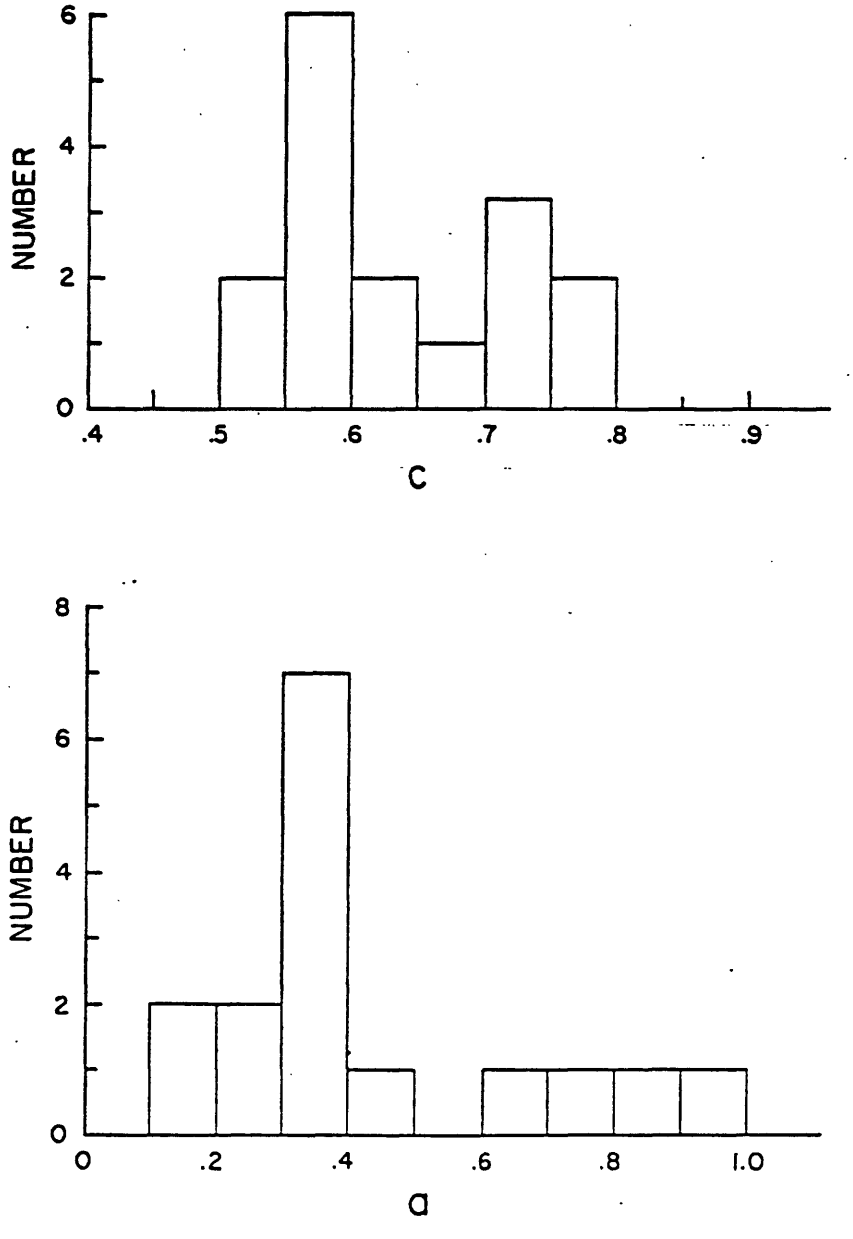

Figure 10.--Histograms of the generalized Cole-Davidson model parameters, a and c, for artifical Ca-montmorillonite glass bead mixtures.

estimated values of the parameters a and c for all spectra measured on artificial samples for which the phase peak was well defined. As can be seen, all of the estimated values of c are greater than 0.5 and most of the values of a are less than 0.5. These results suggest that membrane polarization effects can be physically described by the Madden-Marshall model and empirically described by the generalized Cole-Davidson model. The fact that the observed slopes are not exactly 1.0 and 0.5, as for the Cole-Davidson distribution (fig. 4), could be due to a distribution of length scales associated with a range in grain size of the glass beads used.

Dependence on Grain Size

In order to evaluate the effects of grain size, a series of samples was made in which the weight percent montmorillonite (measured dry) was fixed at 3.0, and the grain size of the glass beads was varied. Figures 6 through 9 display the observed spectra for 0.01m NaCl and the following grain sizes:

fine	4.0 to 12.5 x 10^{-5}m
medium fine	2.05 to 3.5 x 10^{-4}m
medium coarse	2.5 to 5.0 x 10^{-4}m
coarse	1 x 10^{-3}m

The observed spectra were inverted to the generalized Cole-Davidson model with the estimated parameter values given in the figures. The most noticeable effect of increasing the grain size is to shift the relaxation to lower frequency, thus increasing τ. This result indicates that the length scale which controls the time constant is dependent on the size of the glass beads rather than the size of the clay particles, in agreement with results of Vacquier et

al (1957). This would tend to support the Madden-Marshall model in which the time constant is dependent on the distance between selective zones which, for our artificial samples, is presumably controlled by the size of the beads. Figure 11 summarizes the results of varying the grain size for the samples saturated in solutions with differing conductivity. The Madden-Marshall model predicts that would depend on $(L_1)^2$. From figure 11, however, we tend to observe the contradictory result that τ depends on distance to the first power. From figures 1 and 4, a critical distance, L_1, of 3.3×10^{-4}m, would yield a time constant of approximately 13, which is well within an order-of-magnitude of the observed data in figure 11 for the medium grain sizes. Thus, the Madden-Marshall model predicts time constants which are close to observed values for small grain sizes.

Dependence on Solution Conductivity

Figure 12 displays the observed dependence of τ, m, and R_o on solution conductivity, σ_e, for fine and medium-fine grain sizes and 3 percent Ca-montmorillonite by weight. If there was no surface conduction associated with the montmorillonite, the plot of log R_o versus log σ_e would be a straight line with slope of 1.0. The slopes in figure 12 of less than 1.0 for small σ_e are evidence that the clay is contributing to the samples' conductivity. From Waxman and Smits (1972) the component of surface conduction is

$$\sigma_s = F/R_o - \sigma_e,$$

where F is the formation factor. Using the observed values of R_o corresponding to $\sigma_e = 0.027$ and $0.17\ (\Omega - m)^{-1}$, we can calculate σ_s and F, obtaining

$$\sigma_s = 0.10\ (\Omega - m)^{-1}, \qquad F = 2.9,$$

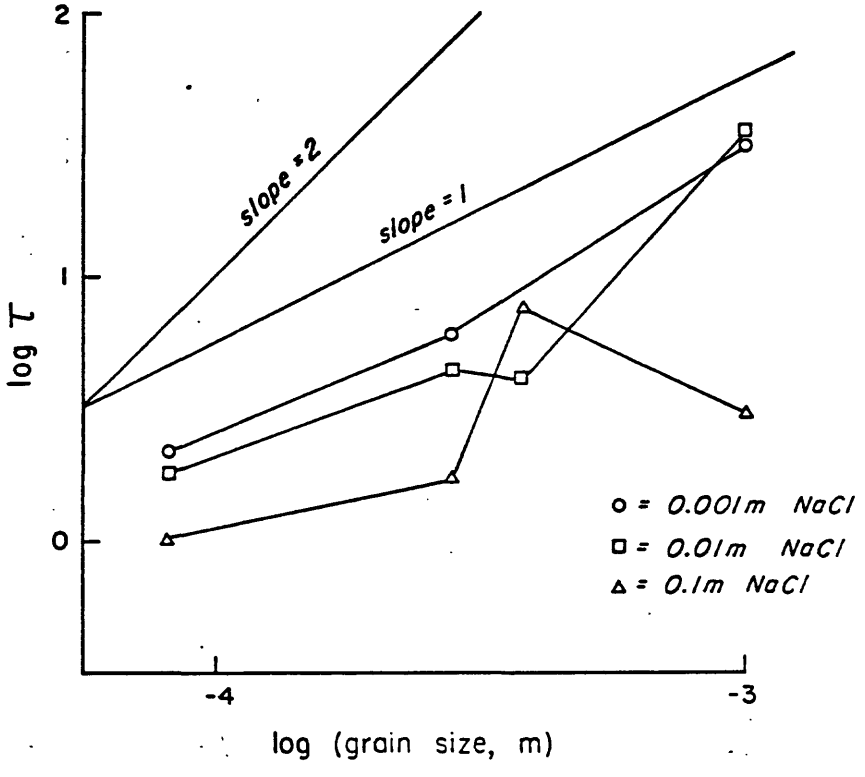

Figure 11.--Observed dependence of time constant, τ, on a glass bead grain size for 3 different NaCl concentrations.

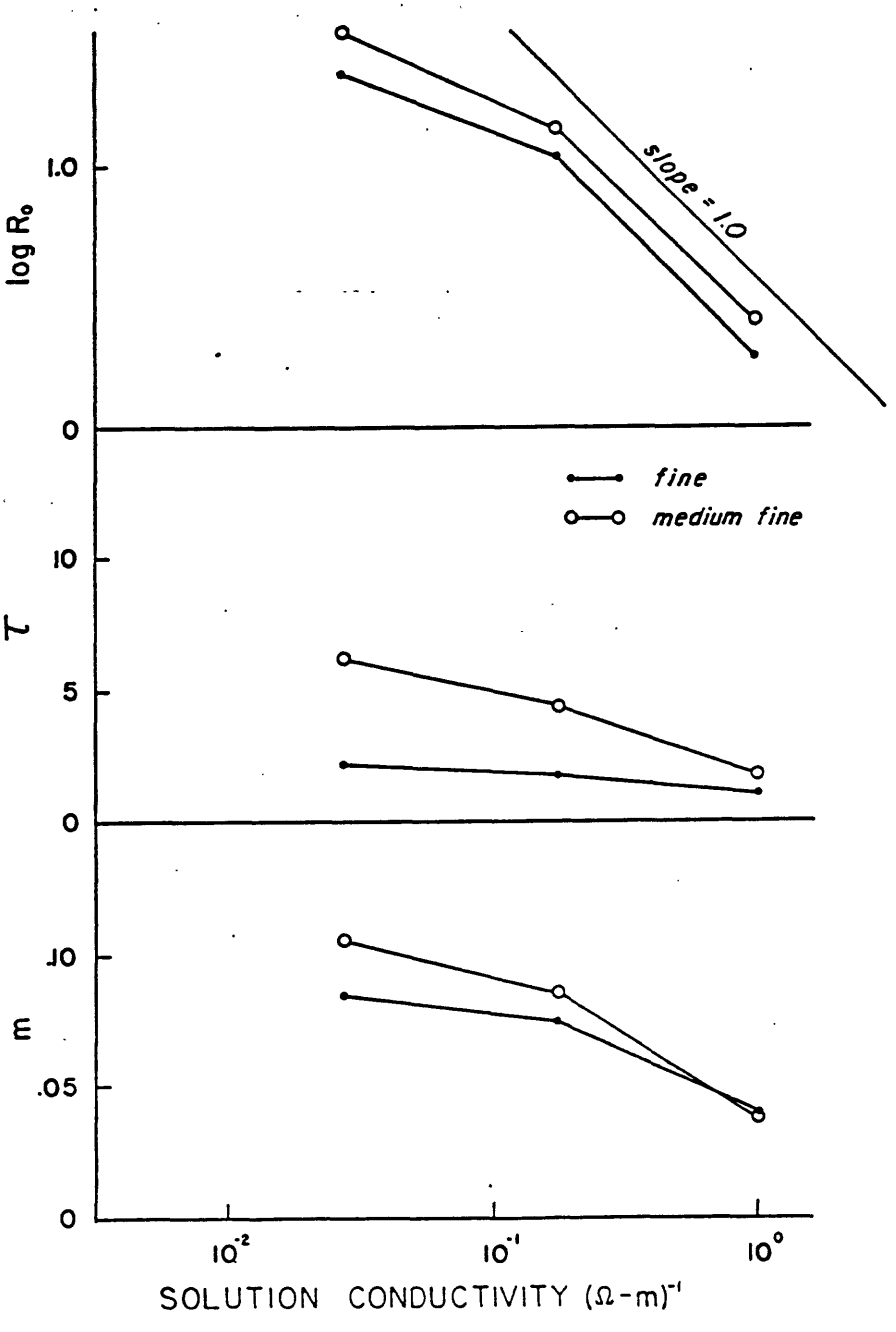

Figure 12.--Observed dependence of background resistivity, time constant, and chargeability on solution conductivity for fine and medium-fine grain sizes.

$\sigma_s = 0.08$, $F = 3.4$,

for fine and medium-fine grain sizes, respectively. Using R_∞ instead of R_o would result in the values

$\sigma_s = 0.11$, $F = 2.8$,

$\sigma_s = 0.09$, $F = 3.1$.

The values of F calculated here are in good agreement with observed values reported by Smith and Stanford (1978) for spherical grains at 40 percent porosity, and imply an Archies law exponent of 1.2. Further comparison of our data to the Waxman-Smits' model shall be made in a later section.

Figure 12 shows a decrease in τ and m, with an increase in σ_e. The change in τ is insignificant compared to changes which would be caused by variations in grain size (fig. 11). The decrease in m is consistent with a shunting of current around clay particles with increased solution conductivity. This effect would not be predicted by the Madden-Marshall model as presented above since it does not include a parallel conduction path.

Dependence on Clay Content

A series of samples was constructed in which the weight-percent Ca-montmorillonite was varied from 1 to 12 percent. The samples were saturated with 0.003m NaCl prior to measurement. Vacquier et al (1957) describe measurements in which polarizability increased with increasing clay content up to 5 to 9 percent. This is in approximate agreement with our results as shown in figure 13, where estimated values of m are plotted versus weight-percent montmorillonite. The rate of increase of m with increasing clay content is possibly linear for small clay content, but then gradually decreases. Accom-

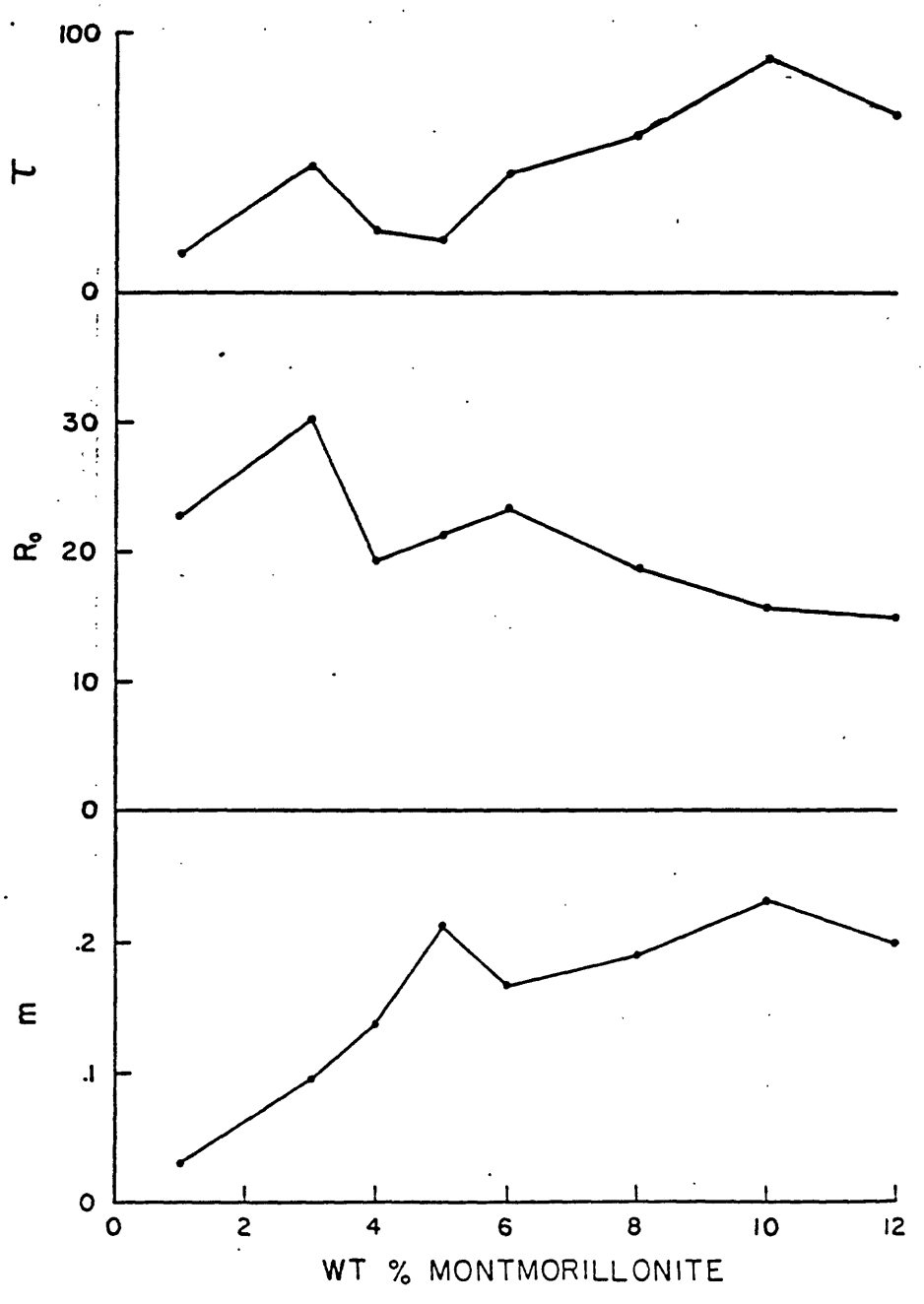

Figure 13.--Observed dependence of time constant, background resistivity, and chargeability on weight percent Ca-montmorillonite.

panying the increase and leveling off of m is a decrease in background resistivity, R_o. The behavior of both m and R_o with increasing clay content can be explained by an increased fraction of the clay forming through-going or interconnected zones. Thesse zones cause a decrease in R_o due to surface conduction, but the clay in them does not significantly contribute to the polarizability. It is apparent that chargeability will be proportional to clay content for only small volume fractions. The effect of clay content on R_o shall be further discussed in the following section.

Figure 13 also shows an increase in time constant, τ, with increase in clay content. In terms of the Madden-Marshall model, this would correspond to an increased distance between selective zones, which does not seem probable.

Comparison to Waxman-Smits Model

We have 2 data sets which are amenable to comparison to the Waxman-Smits model: the results obtained with variation in solution conductivity and results obtained with variation in clay content. According to the Waxman-Smits model, surface conductivity can be expressed as

$$\sigma_s = Q_v B,$$

where Q_v is the CEC per unit pore volume, and B is an empirical parameter which represents the equivalent conductance of the counterions,

$$B = .001\,\lambda\left[1 - a\exp\left(\frac{-\sigma_e}{\gamma}\right)\right],$$

where

σ_e = solution conductivity, $(\text{ohm-m})^{-1}$,

λ = $F\mu$ = equivalent ionic conductance of exchange ions, $m^2/\text{ohm-equiv}$,

F = Faraday constant,

μ = exchange ion mobility,

a, γ = experimentally-determined constants.

Q_v is expressed in units of meq/m^3 and B in units of m^2/ohm-meq. The clay which was used was calcium montmorillonite (CMS STX1) which was obtained from the Source Clays Depository (Clay Minerals Society) and has a CEC of 84.4 meq/100 gms (W. D. Johns, University of Missouri, written commun., 1981).

From the study of the effects of varying NaCl concentration with fine and medium-fine beads, we obtained above estimates of σ_s which vary from 0.08 to 0.11 $(\Omega - m)^{-1}$. These samples contained approximately 2.0 gms of Ca-montmorillonite which would imply a value of Q_v of 9.9 x 10^4 meq/m^3 for 40 percent porosity. This leads to an estimate of B for these samples which ranges from 8.1 to 11.1 x 10^{-7} m^2/ohm-meq.

The study of the effects of varying the clay content with medium-coarse beads provides a convenient means of testing the Waxman-Smits model, which assumes that the B parameter is independent of clay content. From the model, we have

$$B = \frac{F/R - \sigma_e}{Q_v} .$$

Using measured porosities, resistivities, and solution conductivities, and values of Q_v calculated using the clay CEC and amount, B can be calculated as a function of clay content. The results are presented in figure 14, where calculated values of B are plotted versus weight-percent clay using both R_o and R_∞ in the calculations. The values of B plotted for 3 percent clay do not agree with the other data and have been ignored in joining the data points

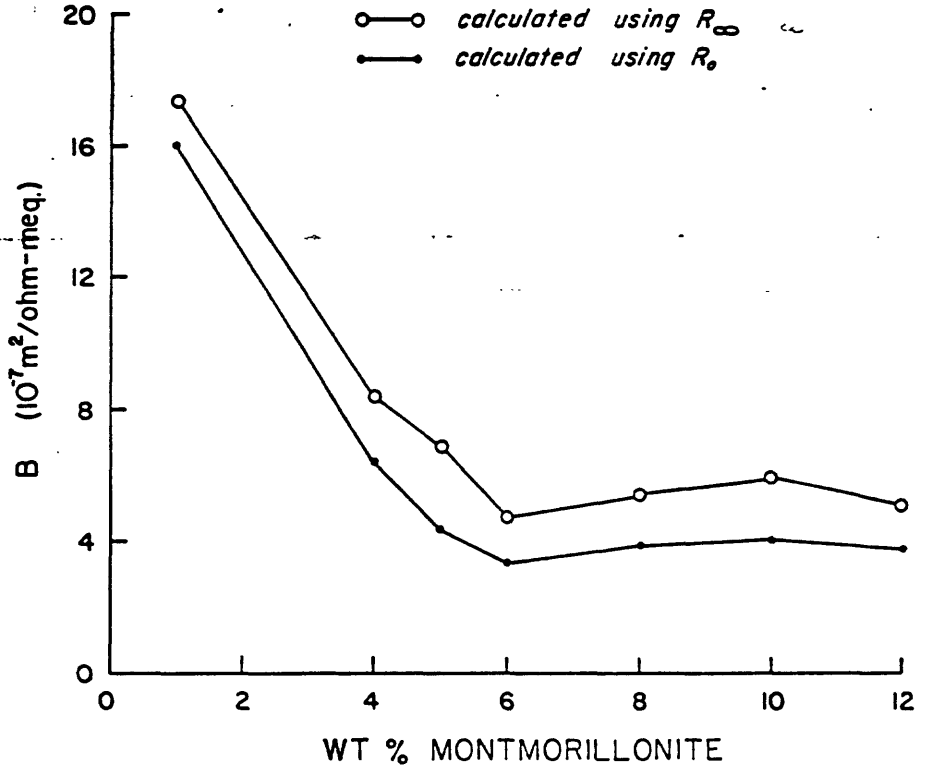

Figure 14.--Values of the Waxman-Smits parameter B, calculated as described in the text, plotted versus weight percent Ca-montmorillonite.

with a line. Note that the estimates of B (8 to 11) obtained in the preceding paragraph for 3 percent clay with fine and medium-fine beads are in good agreement with the other results in figure 14.

Figure 14 indicates the B in the Waxman-Smits model is not constant for our artificial samples with low clay content. The results imply an increase in effective ionic mobility with decreasing clay content. This is opposite to what would be expected if clay particles at low concentration tended to form isolated zones. It is possible that even at 1 percent by weight, the clay particles are close enough for diffuse zones to overlap and for conduction paths to be more-or-less continuous. This is partly substantiated by the resistivity data in figure 13. For 12 Ω-m NaCl solution and 40 percent porosity, resistivity would be 36 ohm-m, which is twice the observed resistivity at 1 percent clay. If these results are taken as representative of natural rocks, then it appears that the Waxman-Smits model is not valid for low clay content.

For clay content greater than 5 to 6 percent, calculated values in figure 14 are approximately constant. It is interesting to compare these values to values reported in Waxman-Smits (1972). They present two groups of estimates of a, γ, and λ obtained from two separate data sets.

	Group 1	Group 2
a	0.83	0.6
γ	2.0	1.3 $(\text{ohm-m})^{-1}$
λ	3.83×10^{-3}	$4.6 \times 10^{-3} m^2/\text{ohm-meq}$
B_{Na} (12 ohm-m)	7.8×10^{-7}	20×10^{-7}
B_{Ca} (12 ohm-m)	3.1×10^{-7}	8×10^{-7}

Measurements by Waxman and Thomas (1976) support Group 1 as being correct. For a 12 ohm-m NaCl solution, values of B calculated according to (3) are given above. These values of B are not applicable to our results, however, since values of λ given above are for Na^+ ions rather than Ca^{++} ions. According to Lorenz (1969), Ca^{++} ions have mobilities on kaolinite which are 40 percent of mobilities of Na^+ ions. If the values of λ given above are reduced by this amount, the second set of B values are obtained, also given above. This second pair of values of B neatly bracket the values of B in figure 14 for high clay content. The best agreement is with the Group 1 values and values of B calculated using R_o.

Dependence on Clay Type

A limited number of measurements were made on artificial samples made with clays other than Ca-montmorillonite. Typical spectra are shown in figures 15 and 16. Figure 15 shows observed spectra for 6 percent by weight Mg, Na-montmorillonite (CEC = 65 meq/100 gms). The estimated chargeability for this sample was only 0.02 compared to 0.16 for a sample with the same weight percent Ca-montmorillonite. These results cannot be explained by differences in CEC's, and are consistent with observations of Vacquier et al (1957). Calcium exchange ions result in greater polarizability than do sodium ions, presumably due to the smaller mobility of calcium on the clay surface as discussed in the preceding section.

Figure 16 presents observed spectra for a sample which was 5 percent weight kaolinite. The material was essentially nonpolarizable, as would be expected for clay with CEC of only 3.3 meq/100 gms.

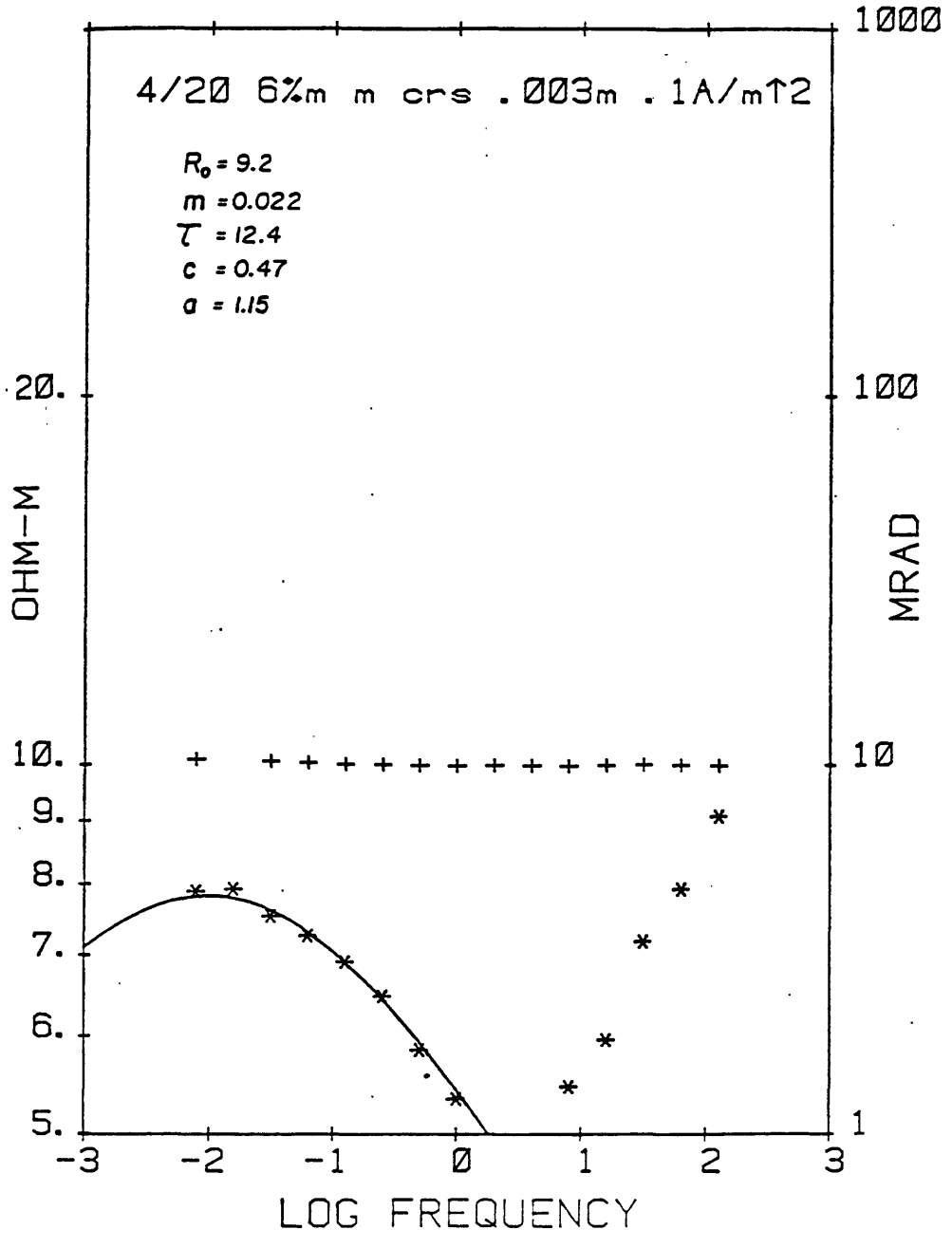

Figure 15.--Observed amplitude and phase for 6 percent by weight Mg, Na-montmorillonite, medium-coarse glass beads, .003m NaCl, 0.1 A/m^2.

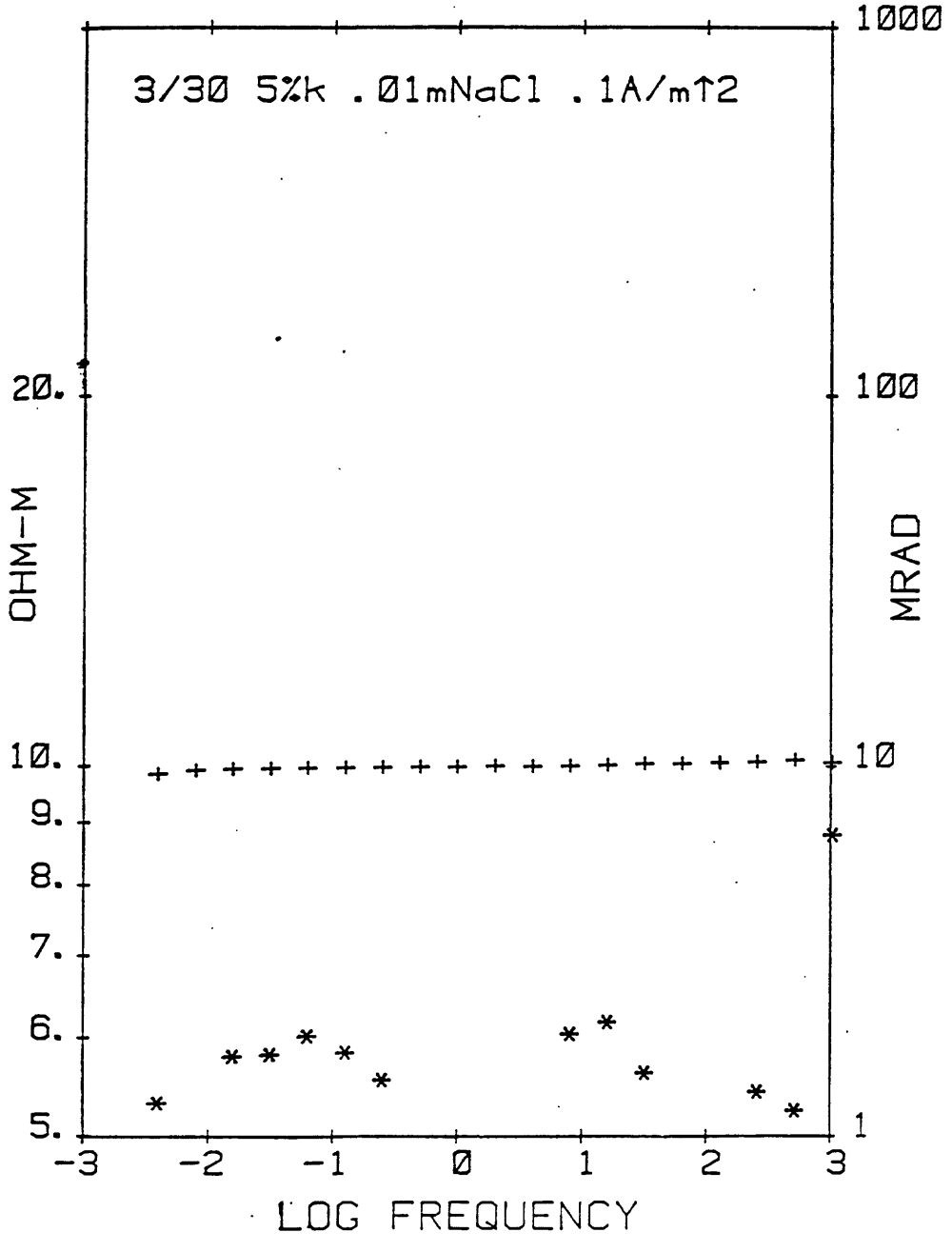

Figure 16.--Observed amplitude and phase for 5 percent kaolinite by weight, 0.01m NaCl, 0.1 A/m^2.

Measurements on Natural Samples

Measurements were made on only a limited number of natural samples of sedimentary origin, and for which there were no mineralogical or textural descriptions available. The observed data for the samples are presented in the Appendix. Samples 985-14 and 985-11B were obtained from Gary Olhoeft (USGS, Denver) and were collected at the Tony M. Mine in Garfield County, Utah, from the Salt Wash Member of the Morrison Formation (Peterson, oral commun., 1980). The samples were obtained from below the water table, and consisted of grey, medium- to fine-grained sandstone, with clay and organic material. There was no pyrite visible with 14x hand lens. Sample 985-14 had a broad phase peak of 6 mrad centered at approximately 1 hz. Sample 985-11B had a noisy and weak phase peak of 2 mrad centered at about the same frequency. Data for sample 985-14 show a high-frequency phase response which is thought to be a spurious effect associated with the measurement system rather than the sample. This high-frequency response, which was observed with most of the natural samples measured, consisted of a rapid increase in phase without an attendant decrease in amplitude. This feature will not be discussed further. Some of the measurements displayed a slight decrease in amplitude at low frequency. This was thought to be due to drift in resistivity with time, since the higher frequency data showed a decrease of similar amount when repeated after the spectra were completed.

Samples Olhoeft 1 through 7 were from a hole logged by Olhoeft (1979). Except for number 6, the samples have little or no polarizability. Sample 7 contained a few percent fine-grained pyrite. The other samples contained no pyrite visible with 14x hand lens.

Sample 1602-21 was a grey, dirty sandstone of unknown origin. It displayed the nicely defined phase peak of approximately 30 mrad centered at 1/32 hz.

The measurements on natural samples cannot be used to test the applicability of the Madden-Marshall or the generalized Cole-Davidson models. This is because the samples are so few in number and because ancillary mineralogical textural data were not available. The data on sample 1602-21 and some of the other samples demonstrate that clay-bearing sandstones can produce low-frequency phase peaks which are consistent in form with peaks obtained with the artificial samples.

NONLINEAR RESPONSE

A secondary objective of this study was to characterize the nonlinear response of clay-bearing materials. The nonlinear response of disseminated sulfide minerals has been examined in detail by Anderson (1981). A comparable study on clays does not exist, although Olhoeft (1977a, 1977b, 1978, 1979) and Olhoeft and Scott (1980) have made observations of nonlinearities associated with clays.

We measure nonlinearity in terms of harmonic distortion of the received voltage waveform in response to a pure sine wave in current. Measurements were made using a ZONGE receiver in conjunction with an HP9825 desk-top calculator. The observed voltage waveform at each frequency was digitized using the ZONGE receiver, and then transferred to the HP9825 where the harmonic content was obtained using cross-correlation techniques. A more complete description of the measurement procedure is available in Anderson (1981). We

report here values of percent harmonic distortion at 2 and 3 times the fundamental frequency,

$$\text{distortion} = \frac{V}{V_o} \times 100 \text{ percent} ,$$

where

V = voltage at 2f and 3f,

V_o = voltage at f,

f = transmitted frequency.

The ZONGE receiver has a 12-bit A to D, so the minimum noise level for our measurements is 1 part in 2^{12}, or 0.024 percent.

In order to compare with clay response, we have conducted a limited number of measurements on a single pyrite interface and with artificial samples of disseminated pyrite. We shall very briefly present the observed data without any further discussion. Observed linear and nonlinear data for a single pyrtie interface are presented in figures 17 and 18. A single interface results in large harmonic distortion which increases with decreasing frequency and for which the 2f harmonics are generally larger than the 3f harmonics. When uniformly-sized grains of pyrite are disseminated in a matrix of glass beads, then a nicely-developed single relaxation is observed (fig. 19). The corresponding nonlinear data, figure 20, show a nicely-developed 2f peak, while the 2f data are essential in the noise level. These data are consistent with data of Anderson (1981). Note in figure 19 that the observed amplitude of low frequency decreases with decreasing frequency. This is similar to observations made with clays, as was discussed previously, and is thought to be due to drift effects rather than any unusual sample response.

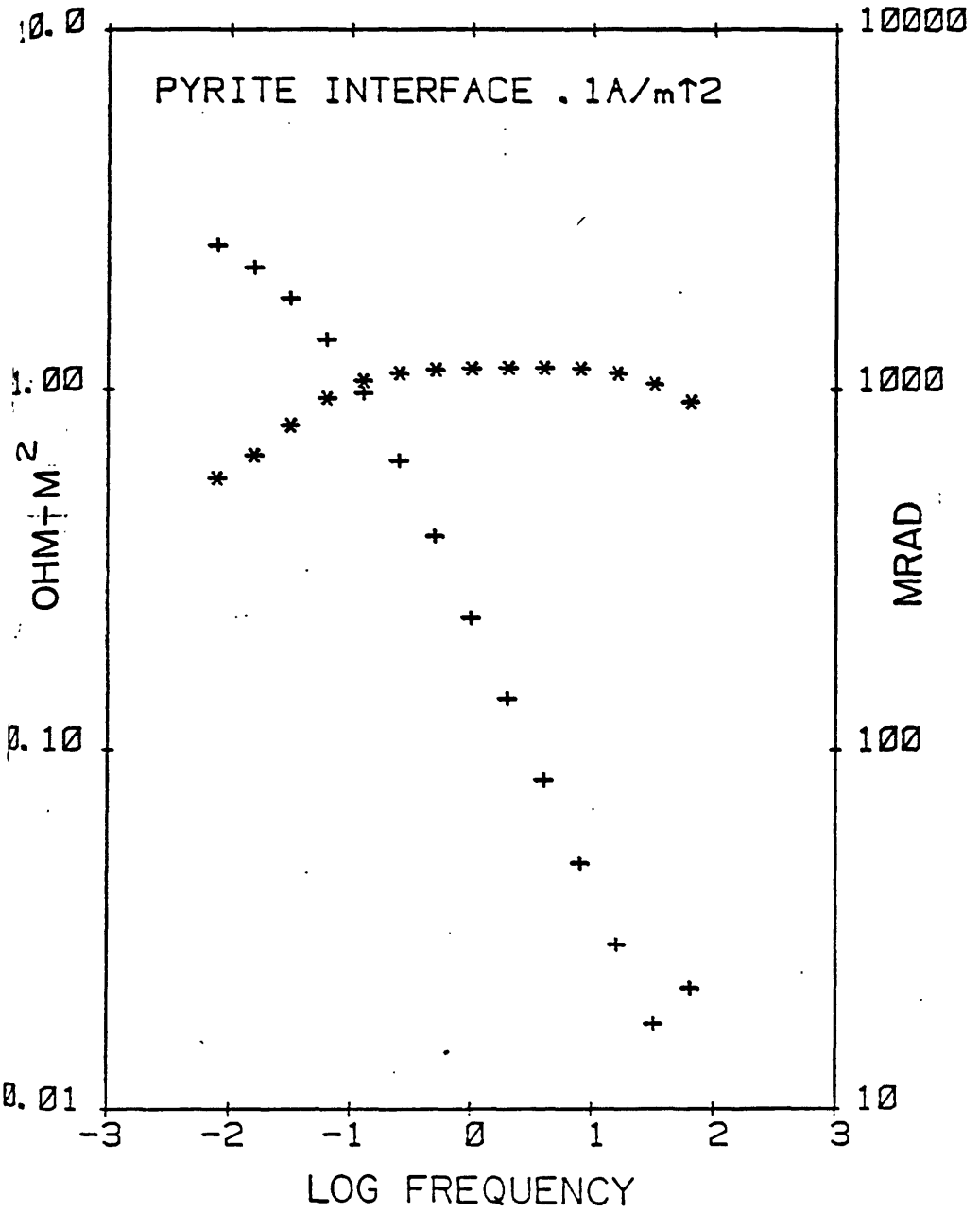

Figure 17.--Observed amplitude and phase for a single pyrite interface, 0.1 A/m^2.

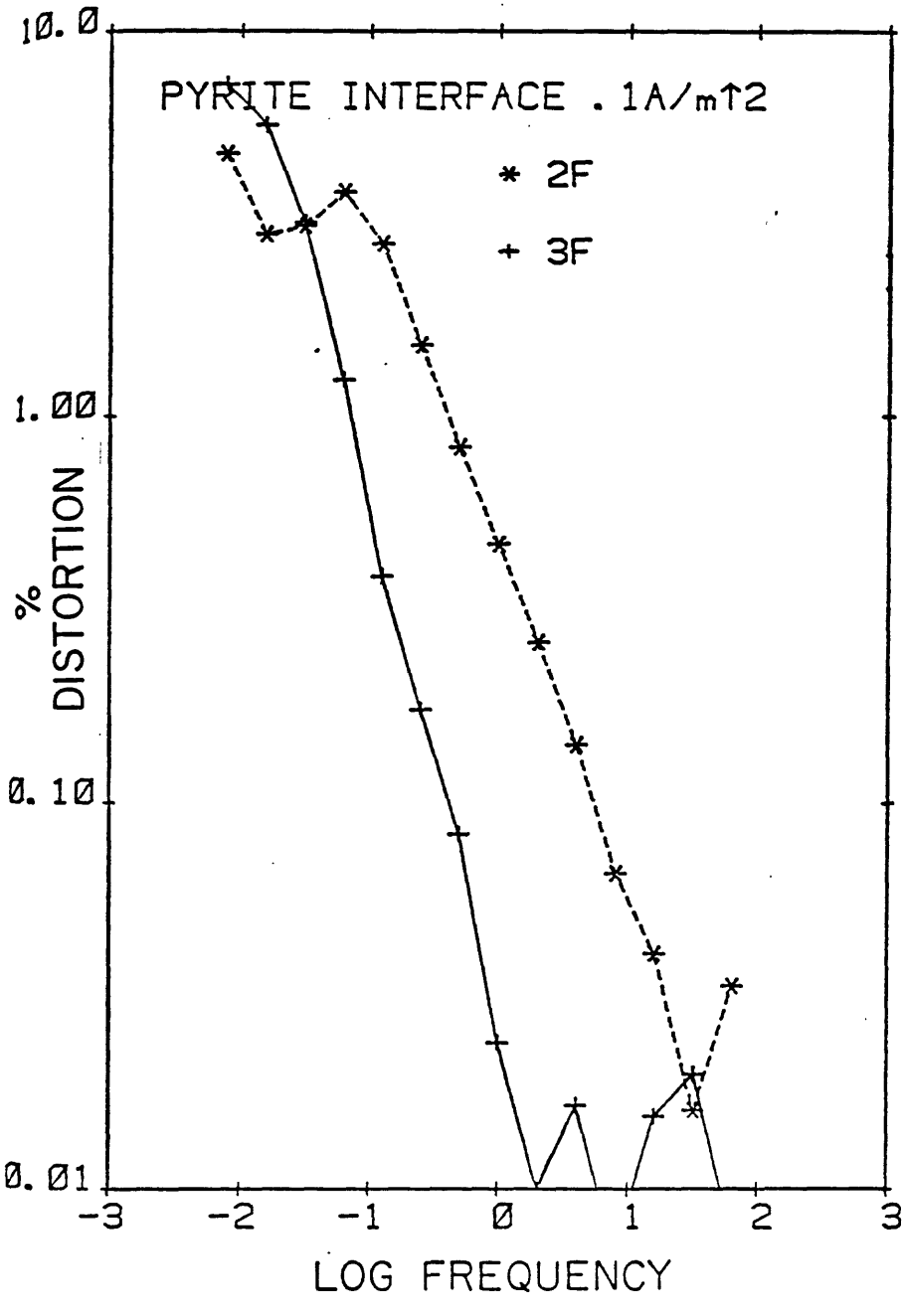

Figure 18.--Observed nonlinear data for a single pyrite interface, 0.1 A/m^2.

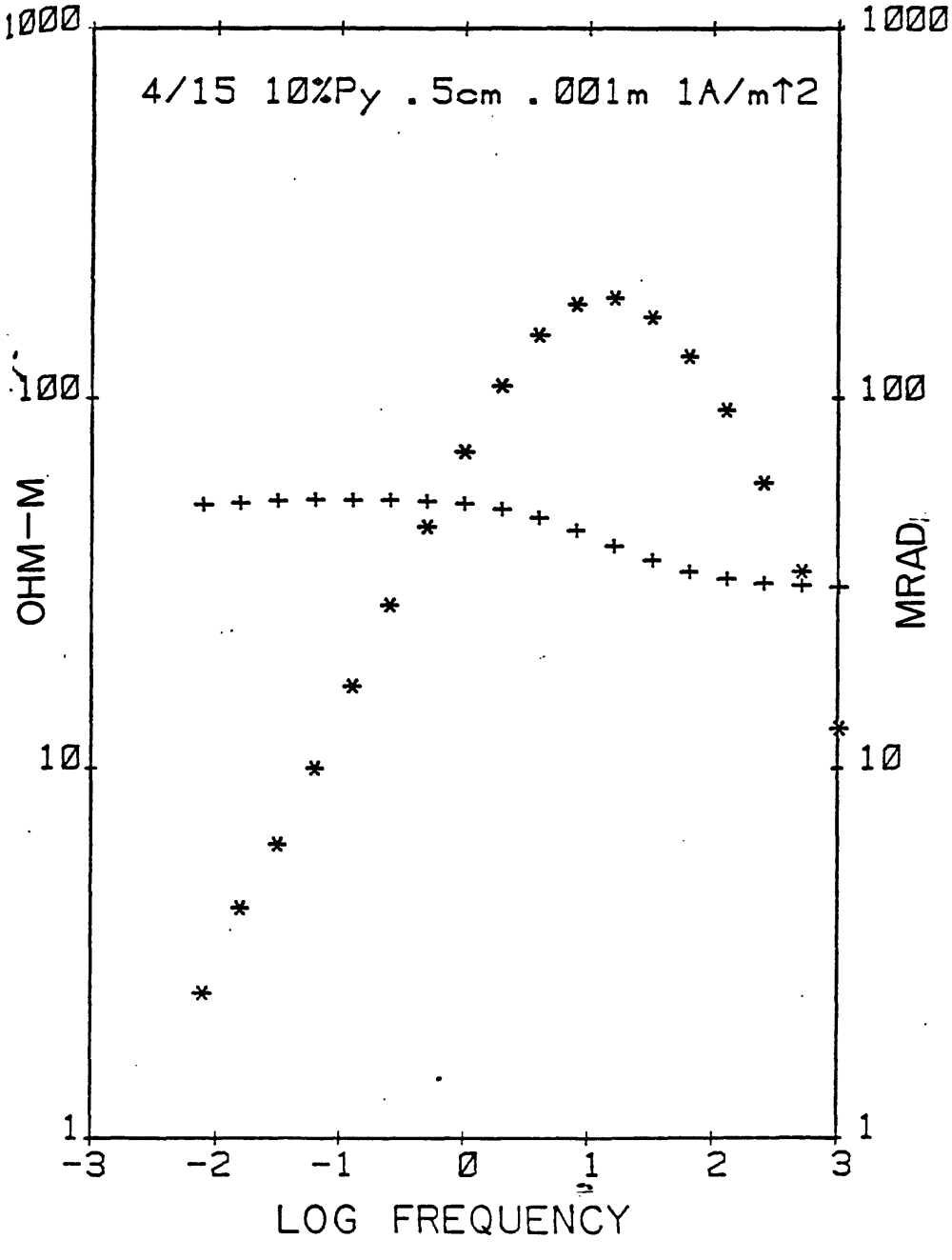

Figure 19.--Observed amplitude and phase for 10 percent pyrite disseminated in glass beads, pyrite grain size of 5 x 10^{-3}m, 0.001m NaCl, 1.0 A/m^2.

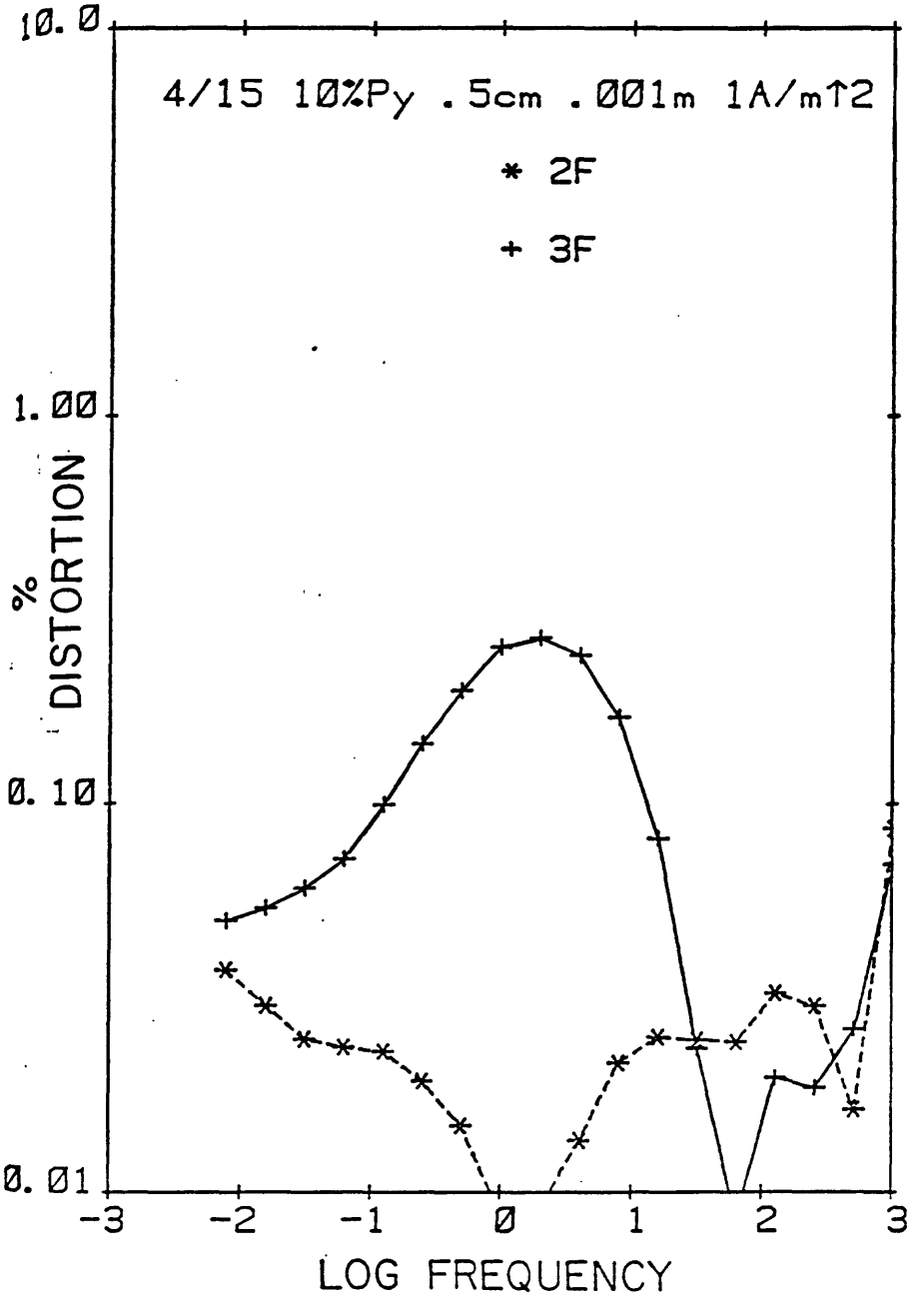

Figure 20.--Observed nonlinear data for 10 percent pyrite disseminated in glass beads, pyrite grain size of 5 x 10^{-3}m, 0.001m NaCl, 1.0 A/m^2.

The observed nonlinear response for clays is simple to describe because nothing was observed which could be ascribed unequivocally to the presence of the clay. Certainly nothing was observed which could be compared to the pyrite resonse. A number of samples of observed data is given in the Appendix. Nothing was observed which could be correlated with membrane polarization for the artifical samples. Sample Olhoeft 6 had response similar to measurements made with a cation-exchange resin with a sharply increasing 3f component at low frequency. Other natural samples showed variable 2f and 3f content which tended to increase with decreasing frequency and was rarely greater then 0.1 percent. This behavior at low frequency is probably due to electrode effects. Figures 21 and 22 display results which are thought to be typical electrode effects for measurements made on two different glass bead blanks with no clay and with two different pairs of Ag/AgCl potential electrodes. The response typically shows 2f and 3f components increasing with decreasing frequency, and the 2f component usually greater than the 3f component. The nonlinear resonse in figure 22 is unusually large, but illustrates that electrode effects can be a major problem while attempting to measure nonlinear properties.

SUMMARY AND CONCLUSIONS

1. Measurements made on artifical samples are consistent with the Madden-Marshall model for membrane polarization.
2. A generalized Cole-Davidson model provides a suitable tool for empirical characterization of observed spectra.

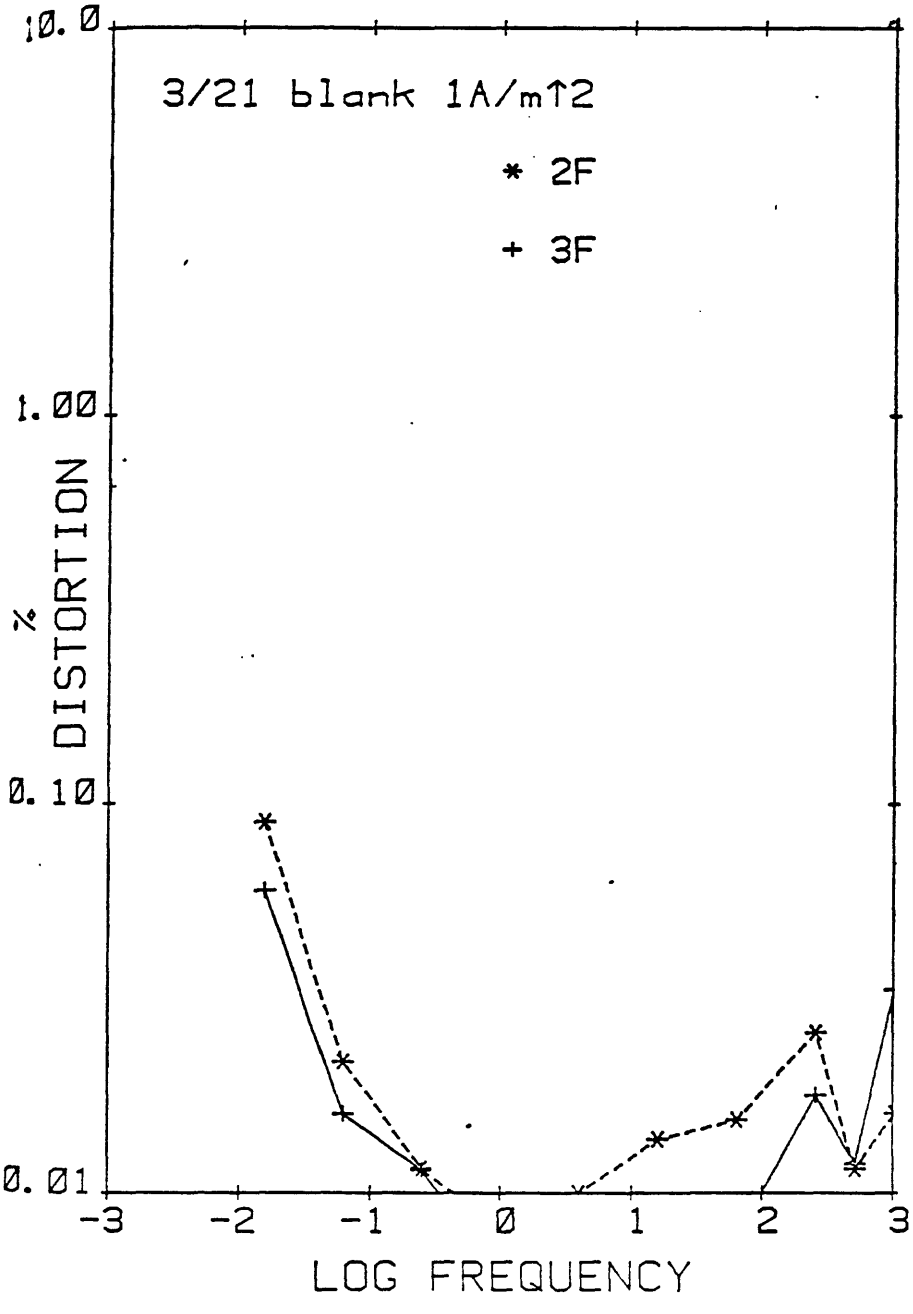

Figure 21.--Observed nonlinear data for glass bead blank, illustrating electrode effects.

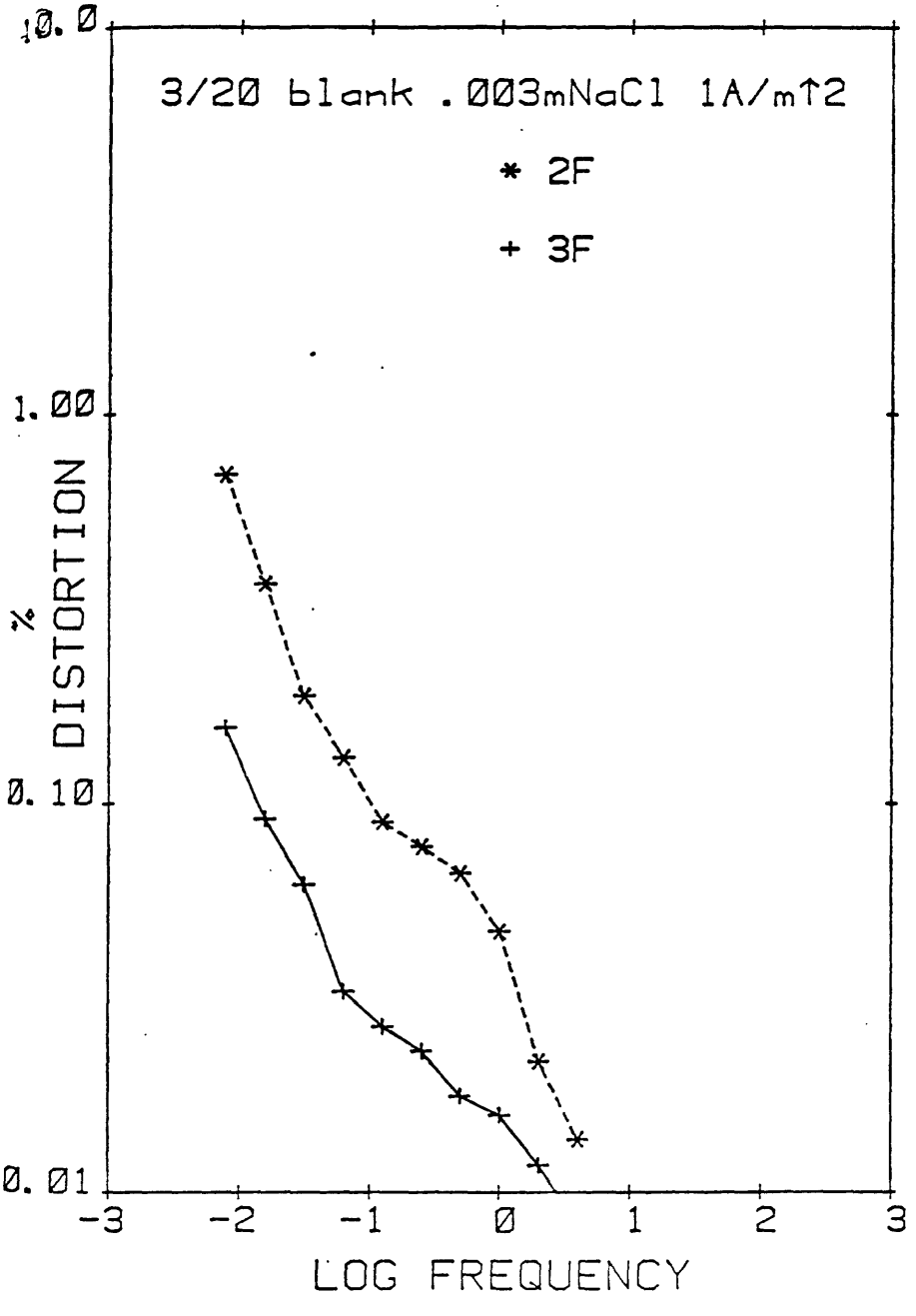

Figure 22.--Observed nonlinear data for glass bead blank, illustrating pronounced electrode effects.

3. Measurements made on artifical samples suggest that the Waxman-Smits model may be invalid for small clay concentration.
4. Measurements made on natural samples are of the same form as those observed with artificial samples, and can be fit with the generalized Cole-Davidson model.
5. No artificial or natural clay-bearing samples were measured which could unequivocally be described as nonlinear.

REFERENCES

Anderson, R., 1981, Nonlinear induced polarization spectra: M.S. thesis, University of Utah, Salt Lake City.

Lorenz, P. B., 1969, Surface conductance and electrokinetic properties of kaolinite beds: Clays and Clay Minerals, v. 17, p. 223-231.

Madden, T. R., and Marshall, D. J., 1959, Induced polarization; a study of its causes and magnitudes in geologic materials: Atomic Energy Commission Report RME-3169.

Olgilvy, A. A., and Kuzmina, E. N., 1972, Hydrogeologic and engineering-geologic possibilities for employing the method of induced potentials: Geophysics, v. 37, p 839-861.

Olhoeft, G. R., 1977a, Nonlinear complex resistivity for the characterization of sedimentary uranium deposits: U.S. Geological Survey Circular 753, p. 12-13.

_____1977b, Nonlinear complex resistivity (abs.): Geophysics, v. 42, p. 1530.

_____1978, Nonlinear complex resistivity in clays (abs.): Geophysics, v. 44, p. 409.

_____1979, Nonlinear electrical properties, in Neel, L., ed., Nonlinear Behavior of Molecules, Atoms, and Ions in Electric, Magnetic, or Electromagnetic Fields: Elsevier, Amsterdam, p. 395-410.

Olhoeft, G. R., and Scott, J. H., 1980, Nonlinear complex resistivity logging: Society of Professional Well-Log Analysts, Transactions 21st Annual Logging Symposium, p. T1-T18.

Pelton, W. H., 1977, Interpretation of induced polarization and resistivity data: Ph.D. dissertation, University of Utah, Salt Lake City.

Roy, K. K., and Elliott, H. M., 1980, Model studies on some aspects of resistivity and membrane polarization behavior over a layered earth: Geophysical Prospecting, v. 28, p. 759-775.

Sill, W. R., 1964, Induced polarization in clay bearing sandstones and the effects of oil saturation: California Research Corporation Report, Institute of Geophysics and Planetary Physics, University of California at San Diego, La Jolla, California.

Smith, D. T., and Dtanford, P. N., 1978, Resistivity-porosity-particle shape relationships for marine sands: Geophysics, v. 43, p. 1250-1268.

Vacquier, V., Holmes, C. R., Kitzinger, P., and Lavengne, M., 1957, Prospecting for ground water by induced electrical polarization: Geophysics, v. 22, p. 660-687.

Waxman, M. H., and Smits, L. J. M., 1972, Electrical conductivities in oil-bearing shaly sands: Society of Petroleum Engineering Journal, Transactions American Institute of Mining Engineers, v. 243, p. 107-122.

Waxman, M. H., and Thomas E. C., 1976, Electrical conductivities in shaly sands. I. The relation between hydrocarbon saturation and resistivity index. II. The temperature coefficient of electrical conductivity: Society of Petrolem Engineering Journal, Transactions American Institute of Mining Engineers, v. 257, p. 213-225.

APPENDIX

Observed Spectra

Natural Samples

Run number	Description
3/9	Sample 985-14, distilled water, 0.1 A/m^2
3/5	Sample 985-11B, measured damp as received in sealed container, 1.0 A/m^2
4/32	Sample Olhoeft 1, 0.1m NaCl, 1.0 A/m^2, depth of 27.9m, porosity = 7.4 percent
4/33	Sample Olhoeft 2, 0.1m NaCl, 1.0 A/m^2, depth of 27.9m, porosity = 9.3 percent
4/35	Sample Olhoeft 3, 0.1m NaCl, 1.0 A/m^2, depth of 29.1m, porosity = 9.8 percent
4/30	Sample Olhoeft 4, 0.1m NaCl, 1.0 A/m^2, depth of 29.8m, porosity = 7.2 percent
4/36	Sample Olhoeft 5, 0.1m NaCl, 1.0 A/m^2, depth of 31.4m, porosity = 39.9 percent
4/37	Sample Olhoeft 6, 0.1m NaCl, 1.0 A/m^2, depth of 34.2m, porosity = 5.3 percent
4/38	Sample Olhoeft 7, 0.1m NaCl, 1.0 A/m^2, depth of 37.0m, porosity = 25.8 percent
3/1	Sample 1602-21, distilled water, 0.1 A/m^2

Artificial Samples

Run number	Description
4/2	3 percent Ca-montmorillonite with fine glass beads, 0.01m NaCl, 0.1 A/m^2, fundamental spectrum in figure 6 in text
4/5	3 percent Ca-montmorillonite with medium-fine glass beads, 0.01m NaCl, 0.1 A/m^2, fundamental spectrum in figure 7 in text
4/4	3 percent Ca-montmorillonite with medium-coarse glass beads, 0.01m NaCl, 0.1 A/m^2, fundamental spectrum in figure 8 in text
4/3	3 percent Ca-montmorillonite with coarse glass beads, 0.01m NaCl, 0.1 A/m^2, fundamental spectrum in figure 9 in text
4/20	6 percent Mg, Na-montmorillonite with medium-coarse glass beads, 0.01m NaCl, 0.1 A/m^2, fundamental spectrum in figure 15 in text
3/30	5 percent kaolinite with glass beads, 0.01m NaCl, 0.1 A/m^2, fundamental spectrum in figure 16 in text

Page 49 follows

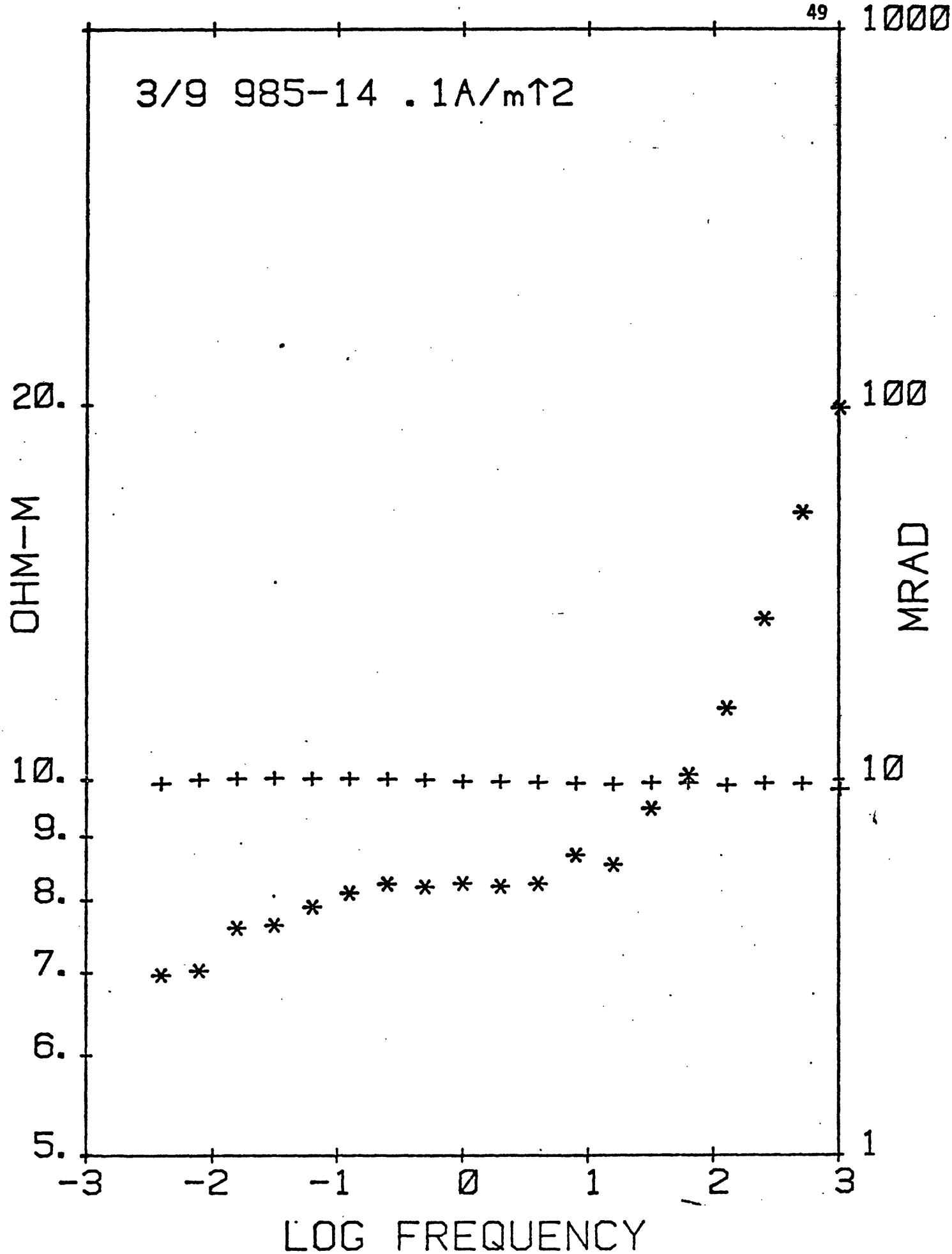
3/9 985-14 .1A/m↑2
1000
100
10
1
20.
10.
9.
8.
7.
6.
5.
OHM-M
MRAD
-3
-2
-1
0
1
2
3
LOG FREQUENCY

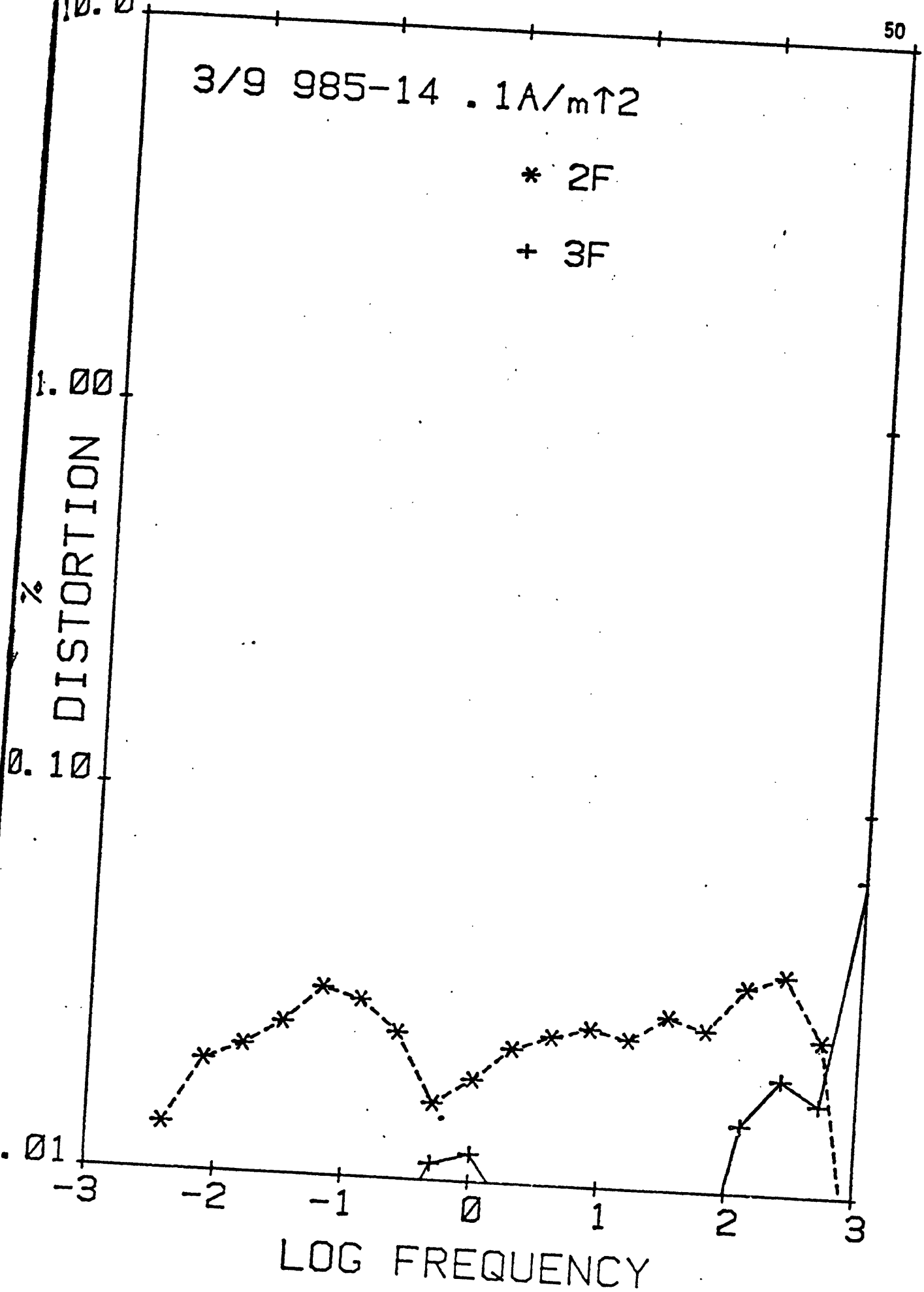
10.0
50
3/9 985-14 .1A/m↑2
* 2F
+ 3F
1.00
% DISTORTION
0.10
.01
-3
-2
-1
0
1
2
3
LOG FREQUENCY

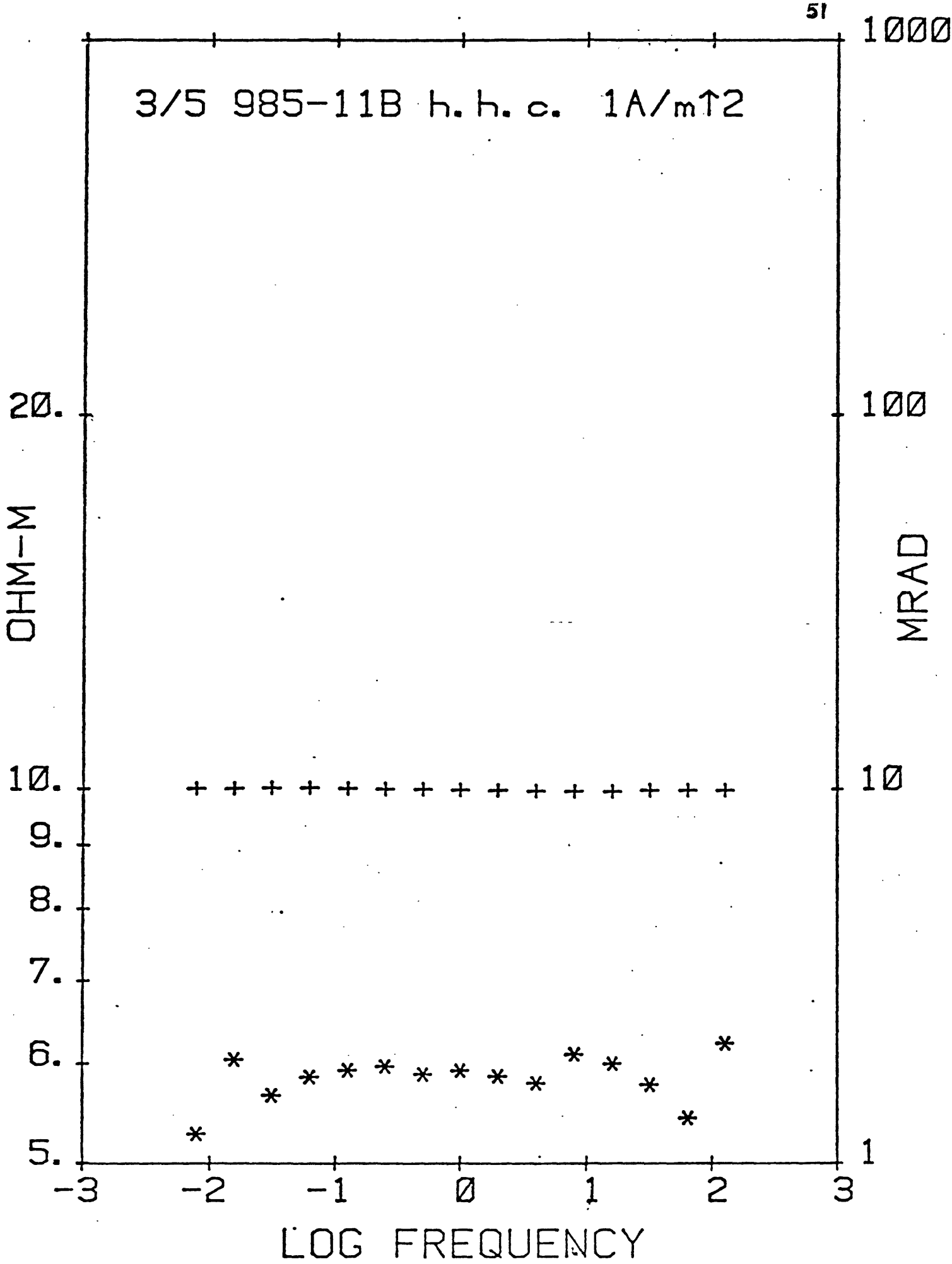
3/5 985-11B h. h. c. 1A/m↑2
1000
20.
100
OHM-M
MRAD
10.
10
9.
8.
7.
6.
5.
1
-3
-2
-1
0
1
2
3
LOG FREQUENCY

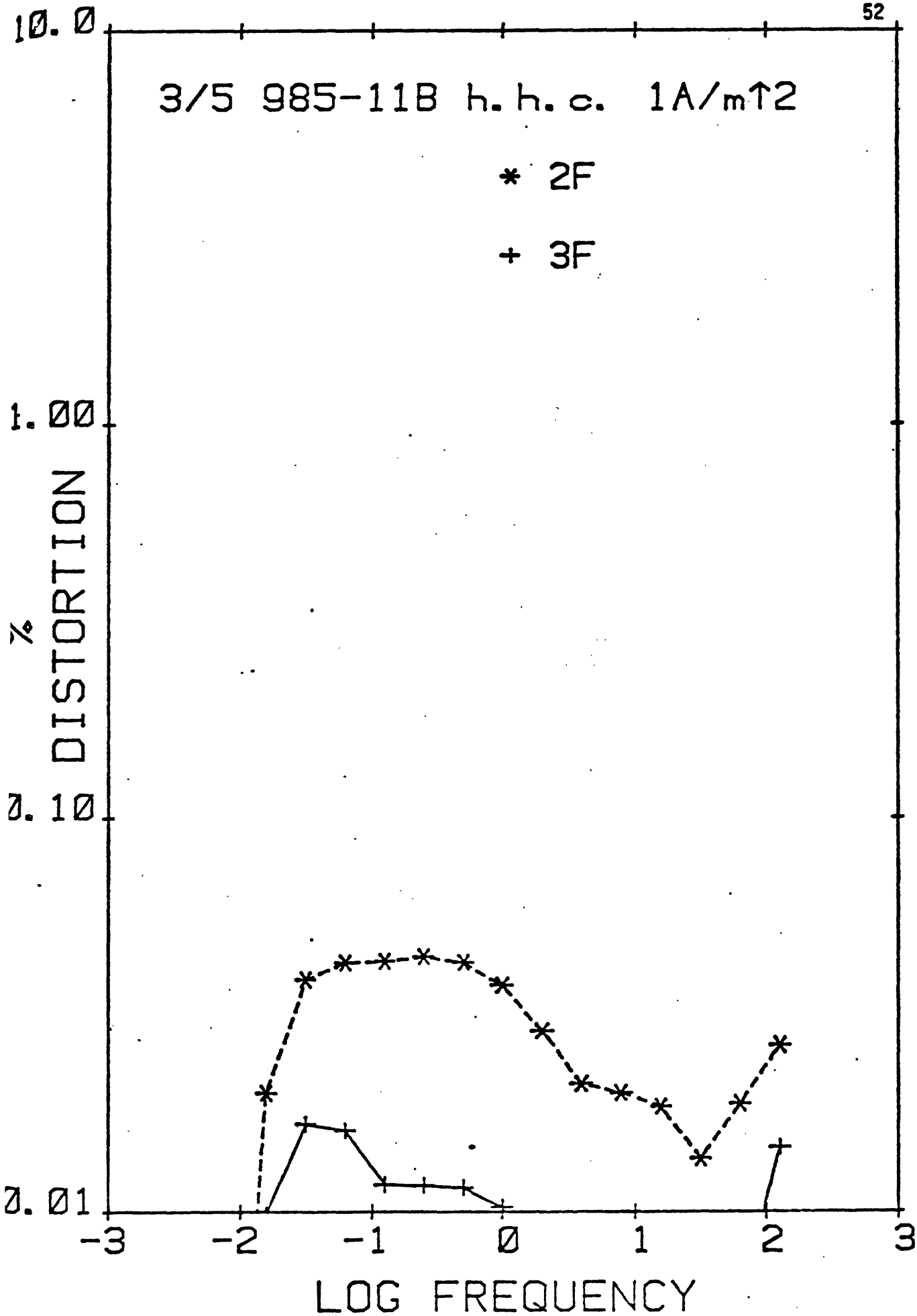
10.0
3/5 985-11B h.h.c. 1A/m↑2
* 2F
+ 3F
1.00
% DISTORTION
0.10
0.01
-3
-2
-1
0
1
2
3
LOG FREQUENCY

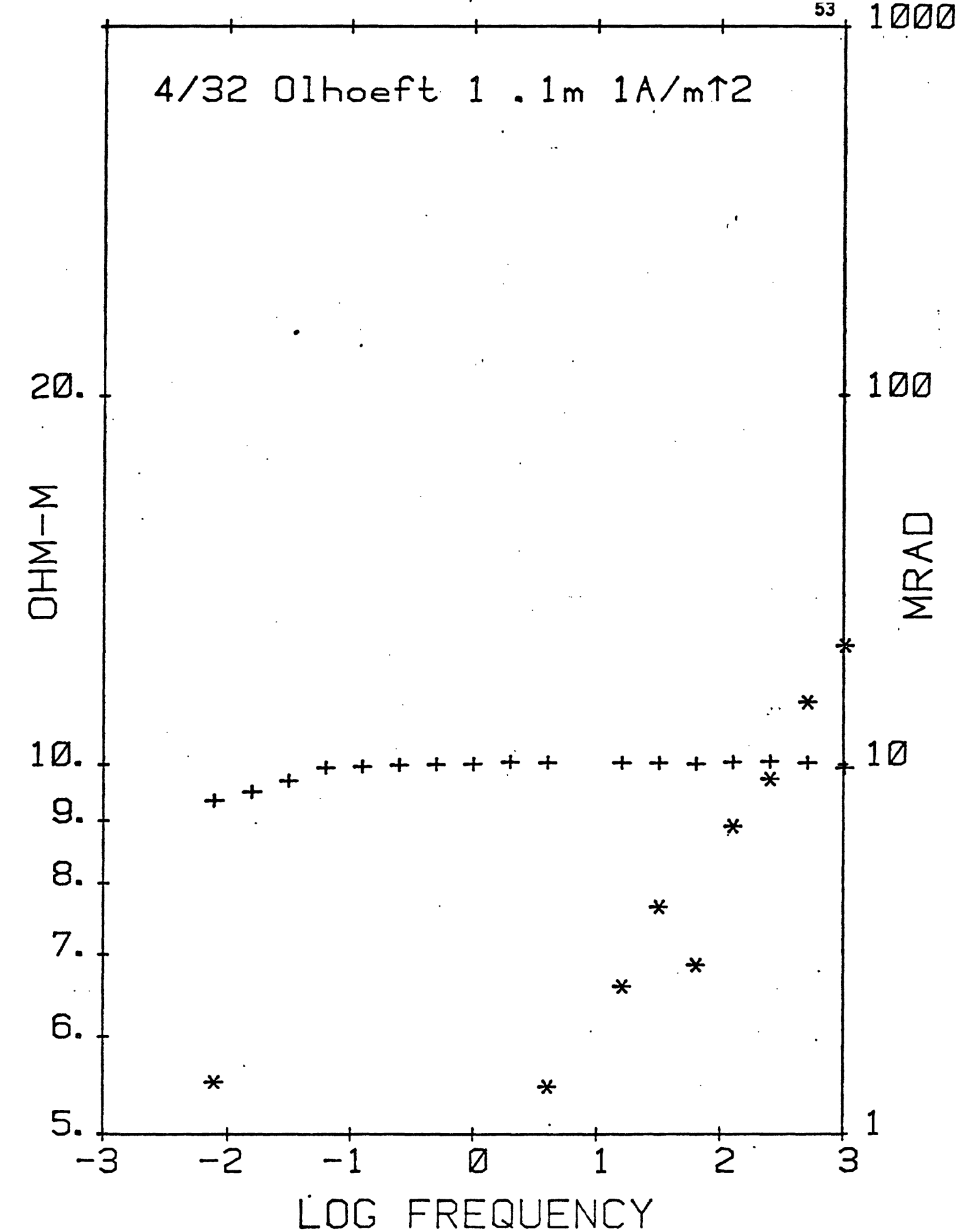
4/32 Olhoeft 1 .1m 1A/m↑2
1000
20.
100
OHM-M
MRAD
10.
10
9.
8.
7.
6.
5.
1
-3
-2
-1
0
1
2
3
LOG FREQUENCY

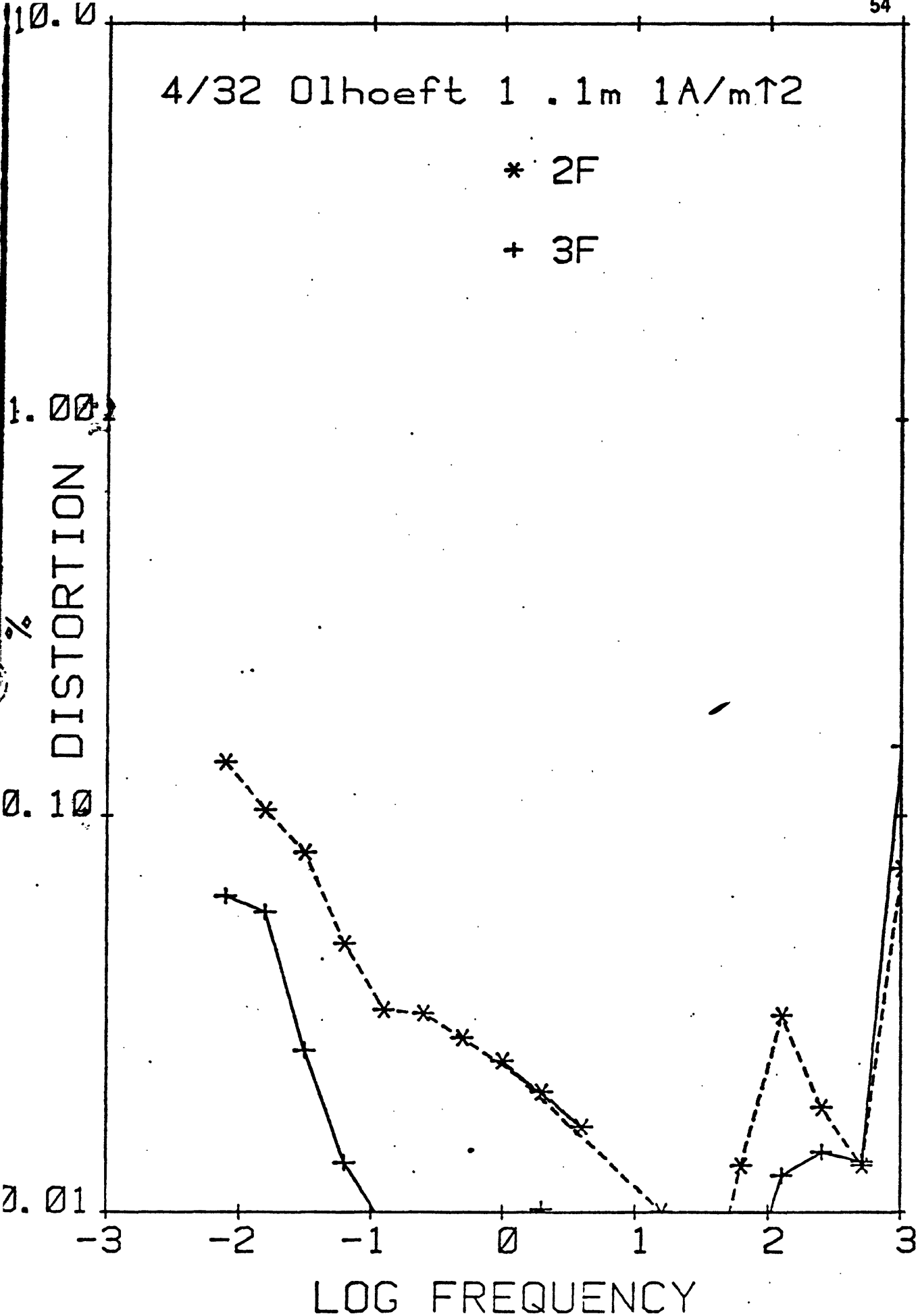
4/32 Olhoeft 1 .1m 1A/m↑2
* 2F
+ 3F
10.0
1.00
% DISTORTION
0.10
0.01
-3
-2
-1
0
1
2
3
LOG FREQUENCY

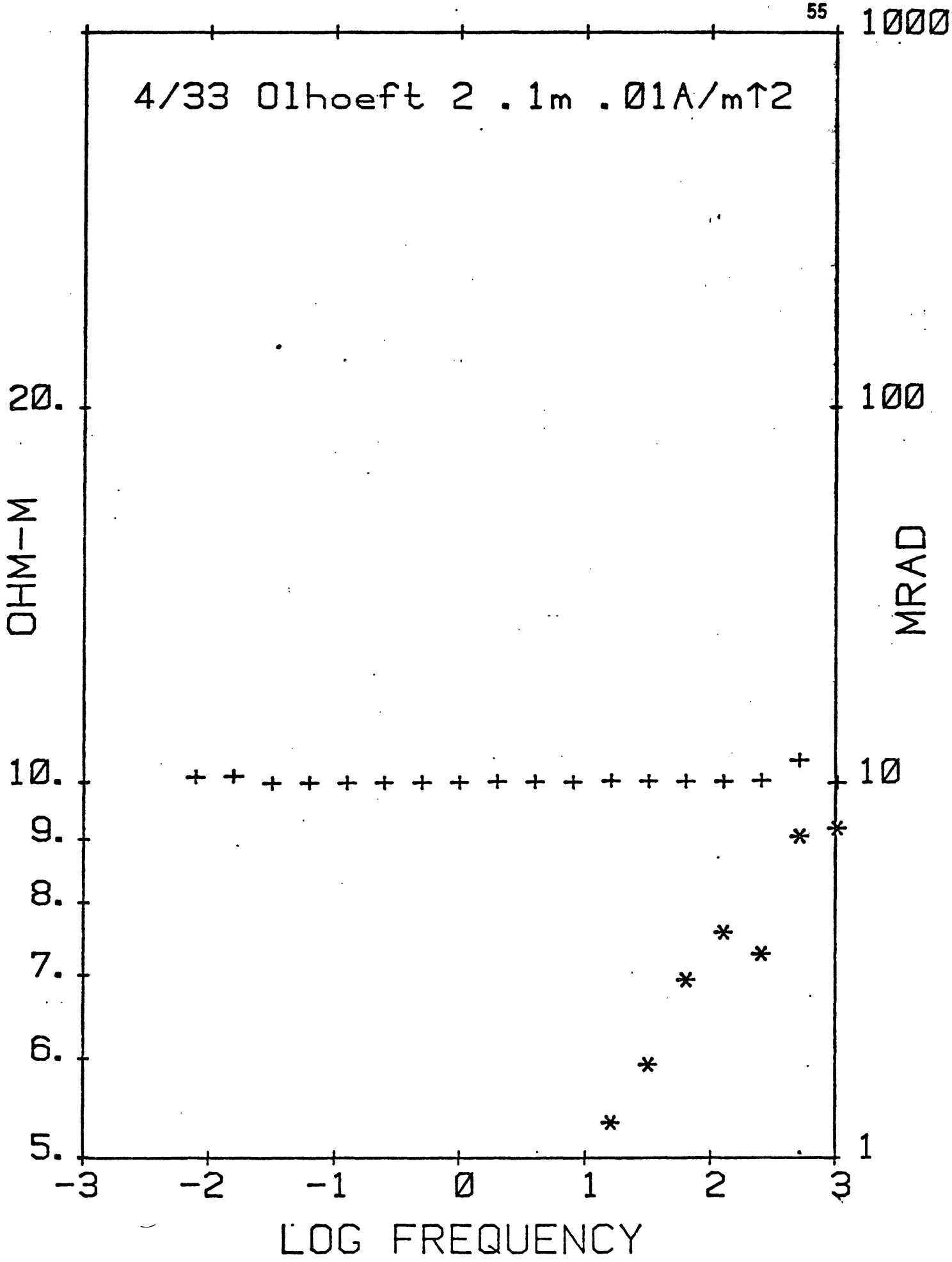
4/33 Olhoeft 2 .1m .01A/m↑2
OHM-M
MRAD
20.
10.
9.
8.
7.
6.
5.
100
10
1
1000
-3
-2
-1
0
1
2
3
LOG FREQUENCY

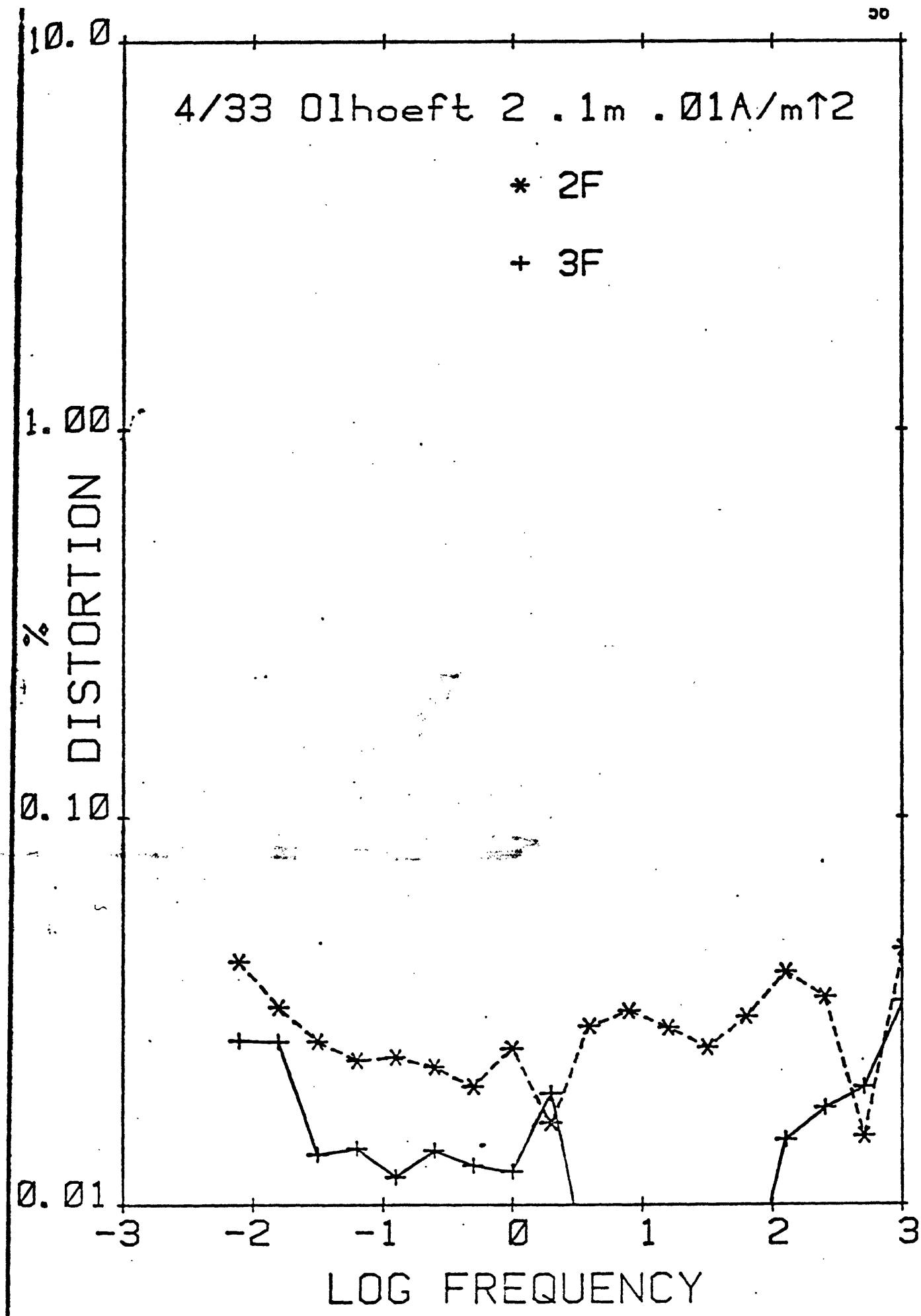
4/33 Olhoeft 2 .1m .01A/m↑2
* 2F
+ 3F
10.0
1.00
0.10
0.01
% DISTORTION
-3
-2
-1
0
1
2
3
LOG FREQUENCY

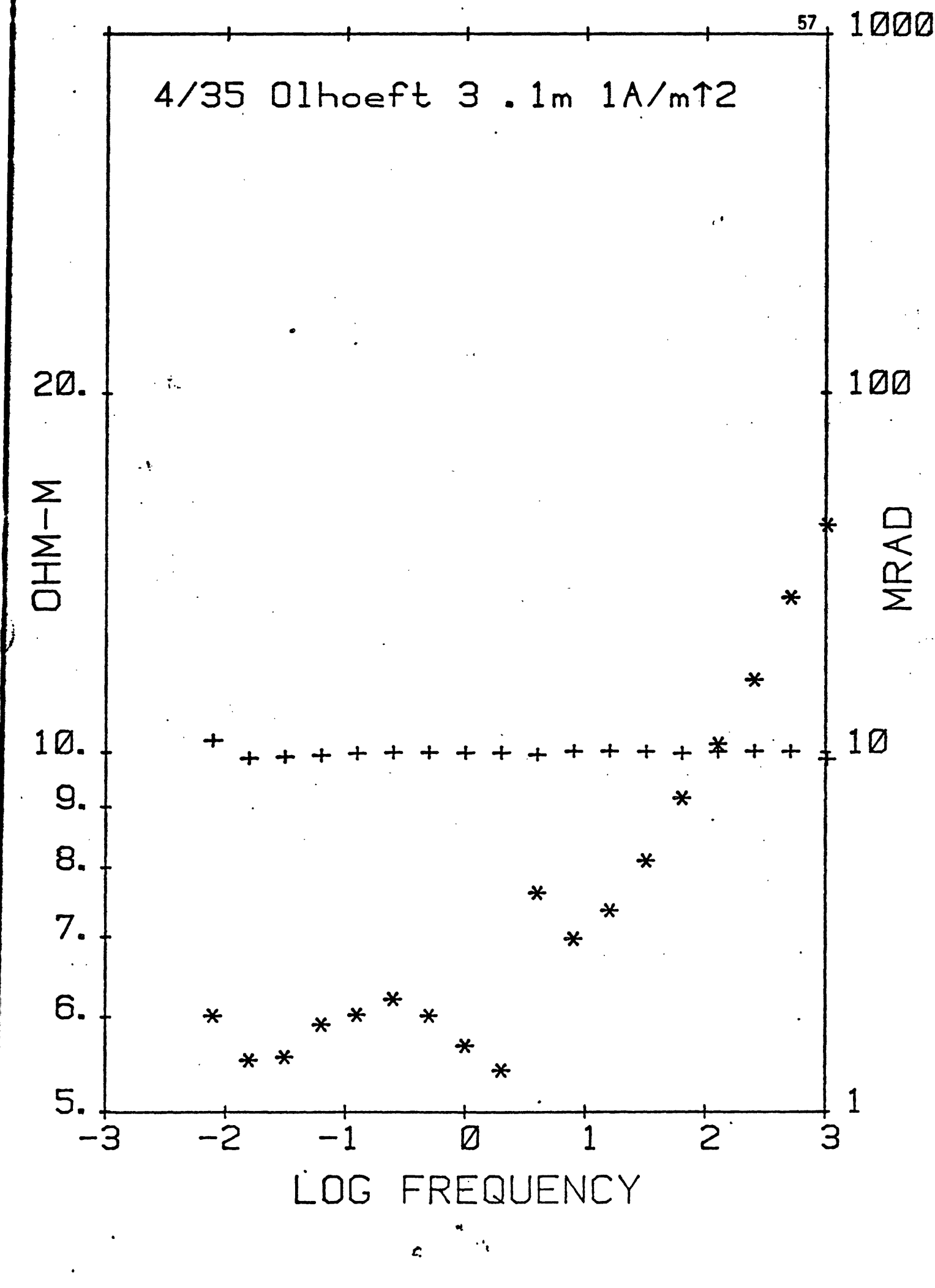
4/35 Olhoeft 3 .1m 1A/m↑2
1000
20.
100
OHM-M
MRAD
10.
10
9.
8.
7.
6.
5.
1
-3
-2
-1
0
1
2
3
LOG FREQUENCY

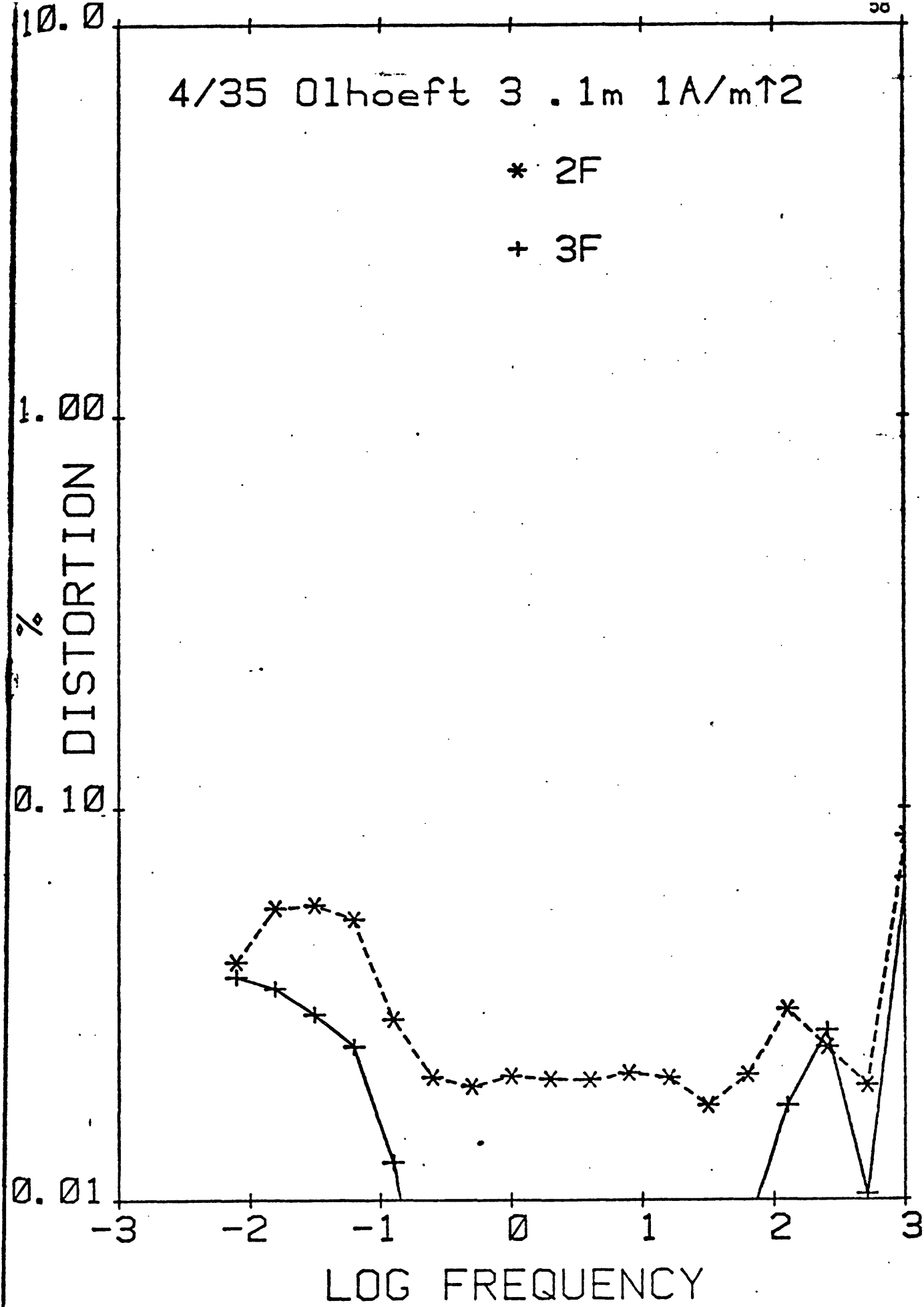
4/35 Olhoeft 3 .1m 1A/m↑2
* 2F
+ 3F
10.0
1.00
0.10
0.01
% DISTORTION
-3
-2
-1
0
1
2
3
LOG FREQUENCY

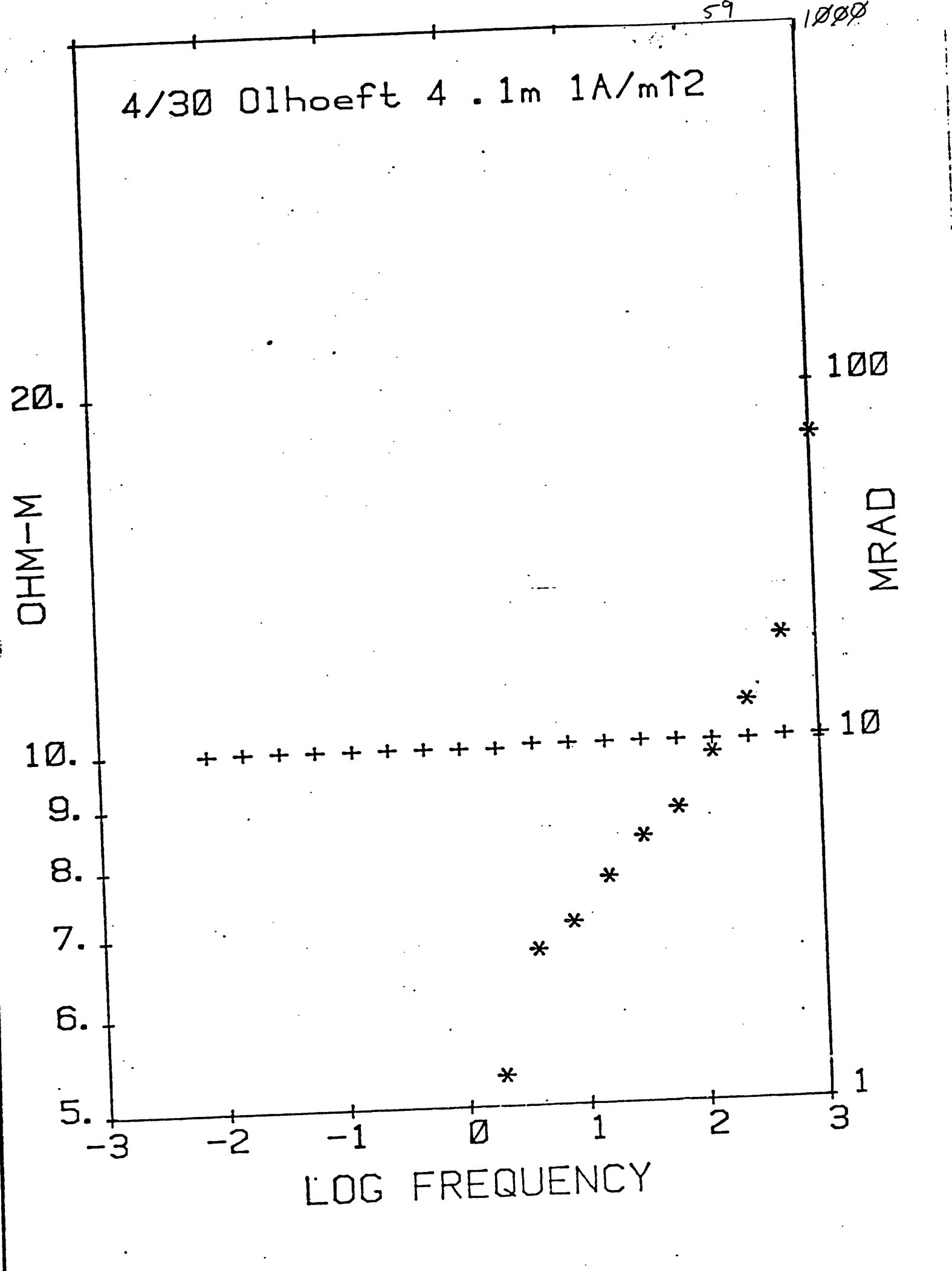
59
1000
4/30 Olhoeft 4 .1m 1A/m↑2
20.
10.
9.
8.
7.
6.
5.
OHM-M
100
10
1
MRAD
-3
-2
-1
0
1
2
3
LOG FREQUENCY

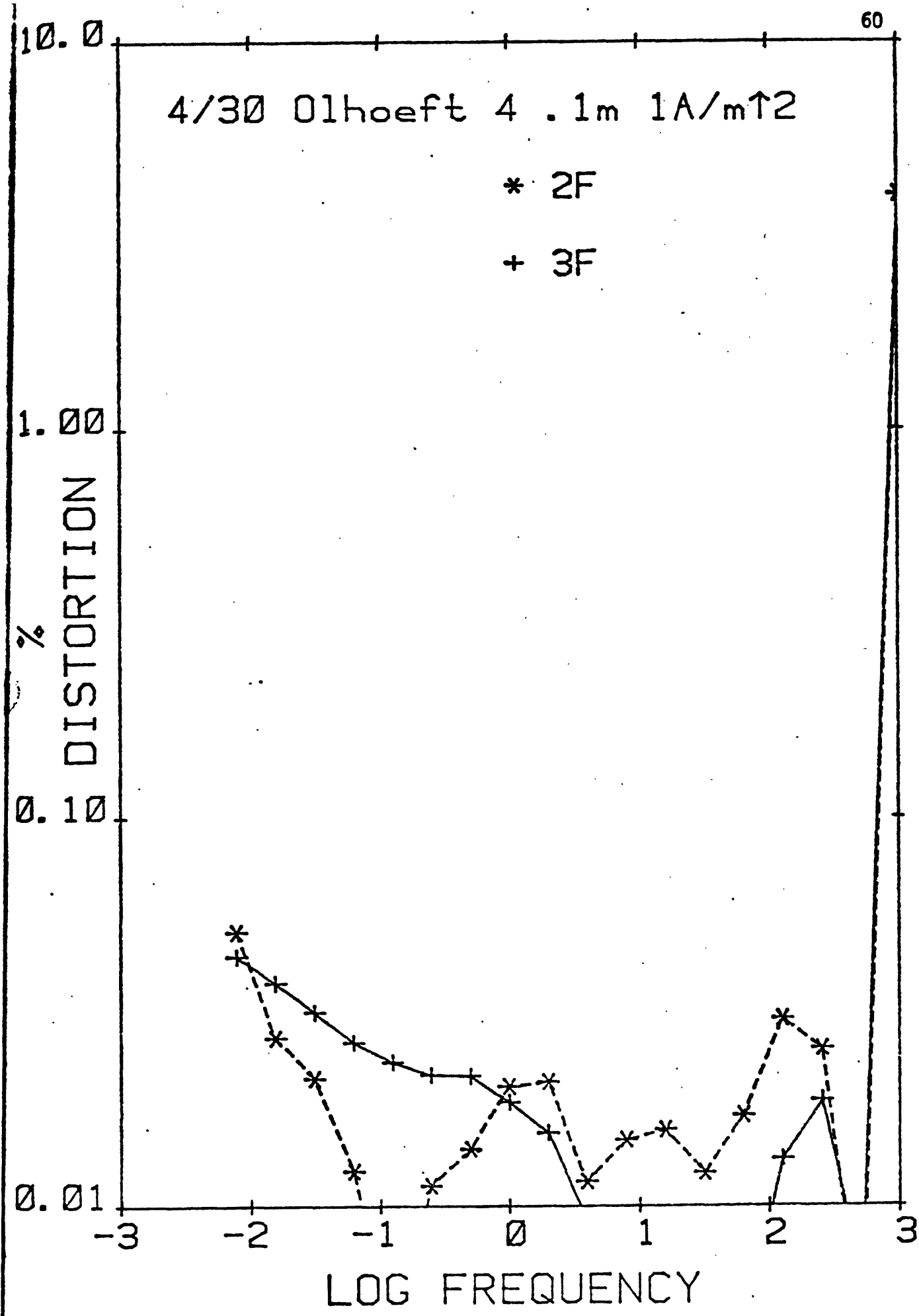
4/30 Olhoeft 4 .1m 1A/m↑2
* 2F
+ 3F
10.0
1.00
0.10
0.01
% DISTORTION
-3
-2
-1
0
1
2
3
LOG FREQUENCY

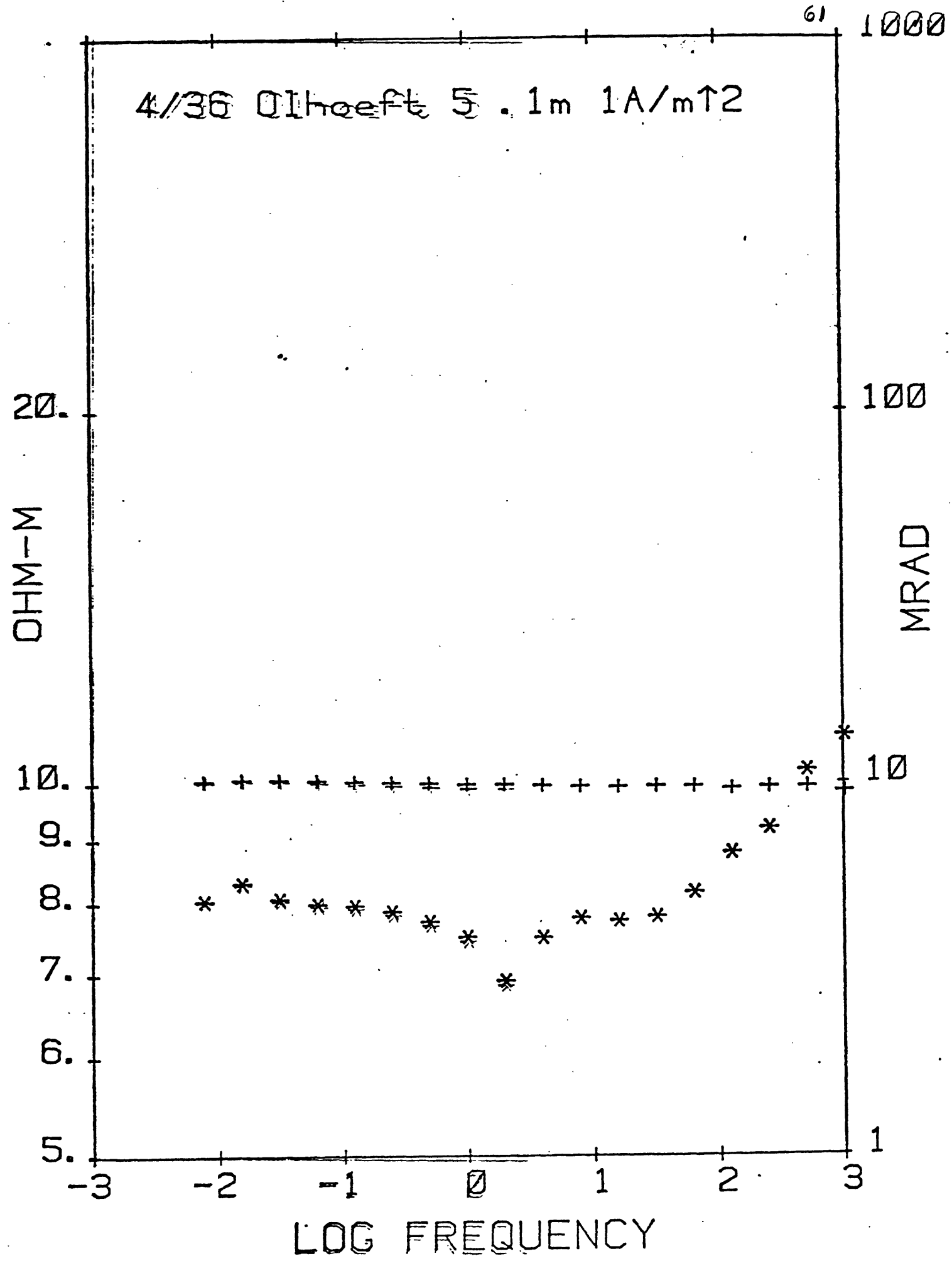
4/36 Oilhoeft 5 .1m 1A/m↑2
1000
100
10
1
20.
10.
9.
8.
7.
6.
5.
OHM-M
MRAD
-3
-2
-1
0
1
2
3
LOG FREQUENCY

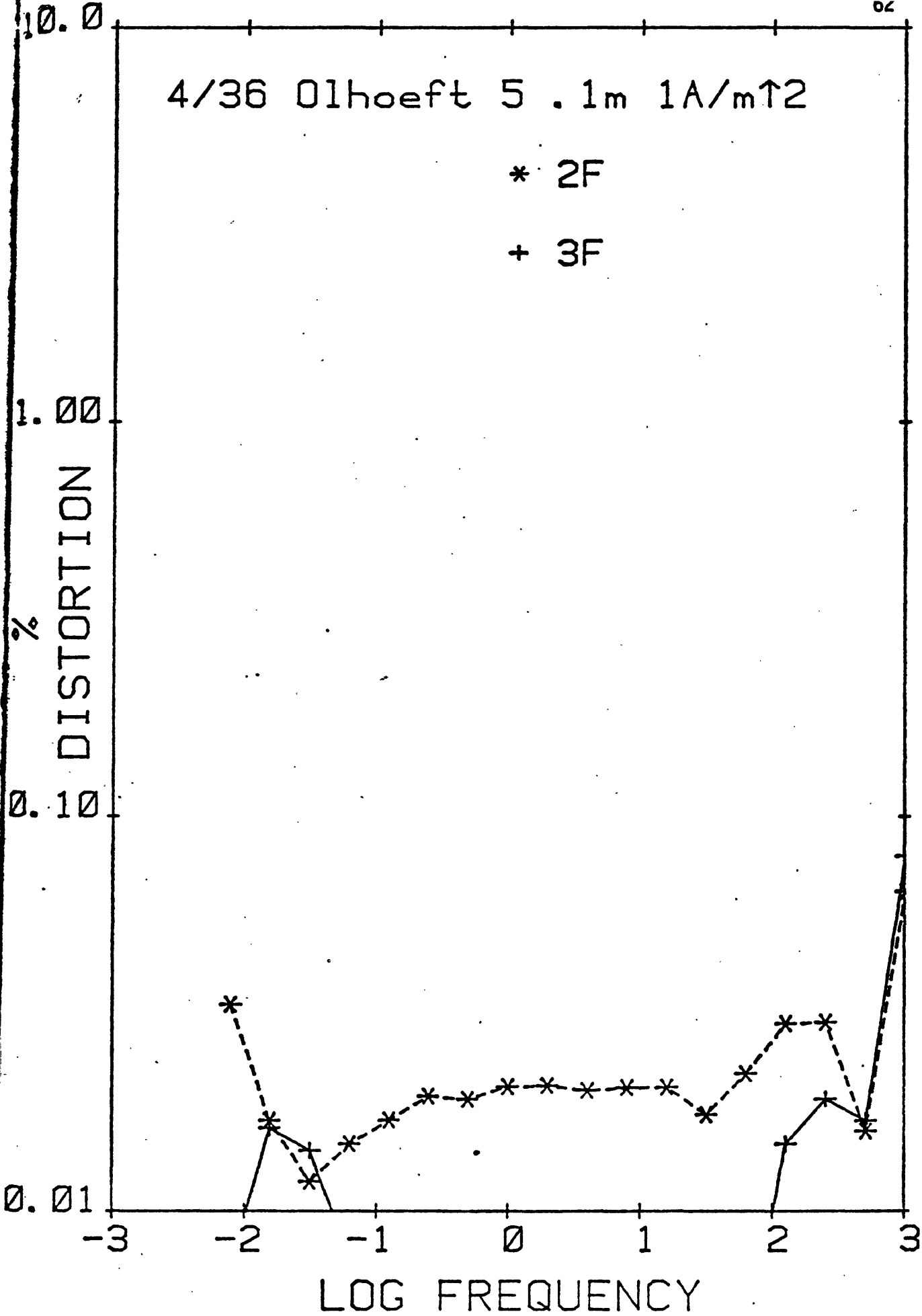
4/36 Olhoeft 5 .1m 1A/m↑2
* 2F
+ 3F
10.0
1.00
0.10
0.01
% DISTORTION
-3
-2
-1
0
1
2
3
LOG FREQUENCY

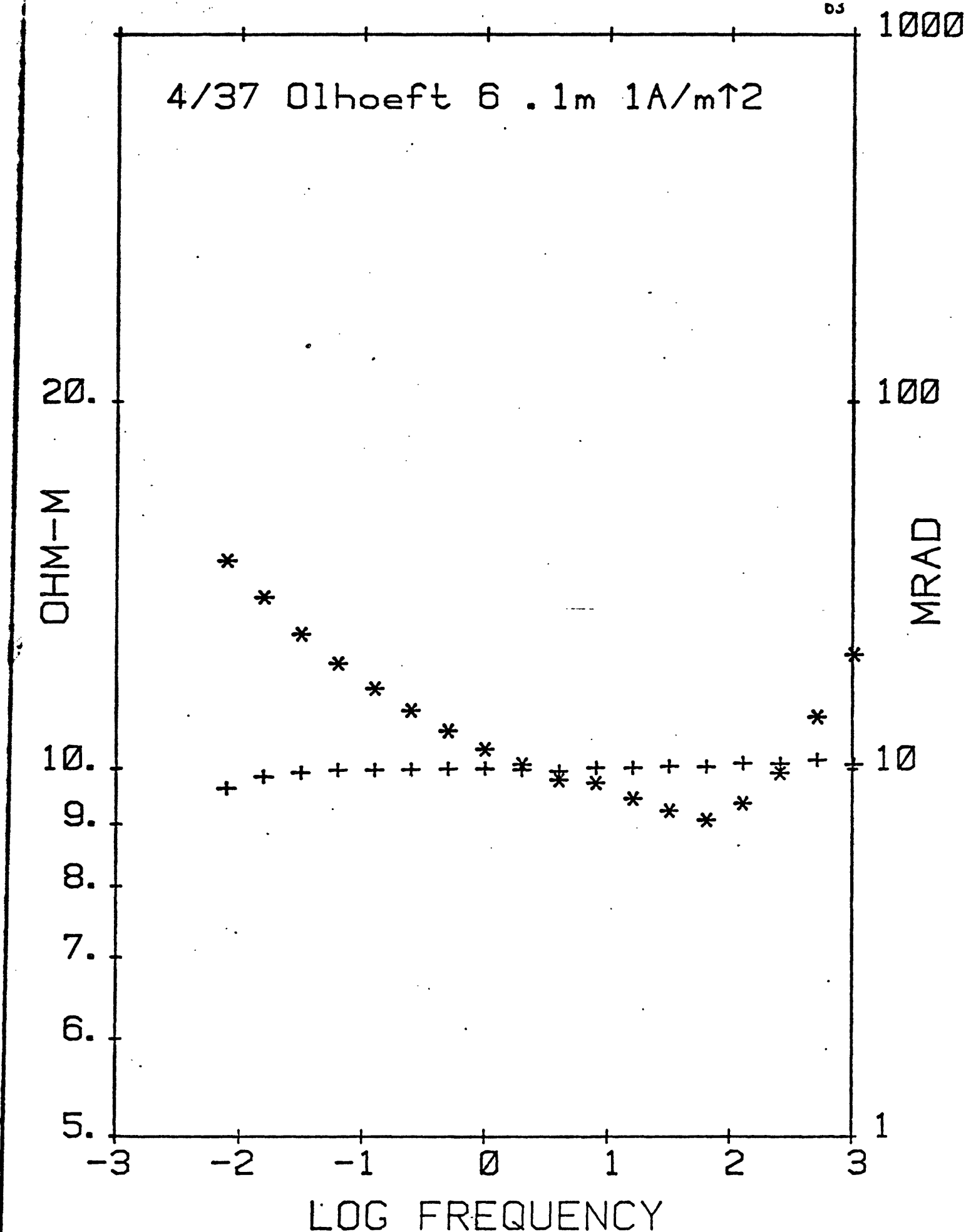
4/37 Olhoeft 6 .1m 1A/m↑2
1000
20.
100
OHM-M
MRAD
10.
10
9.
8.
7.
6.
5.
1
-3
-2
-1
0
1
2
3
LOG FREQUENCY

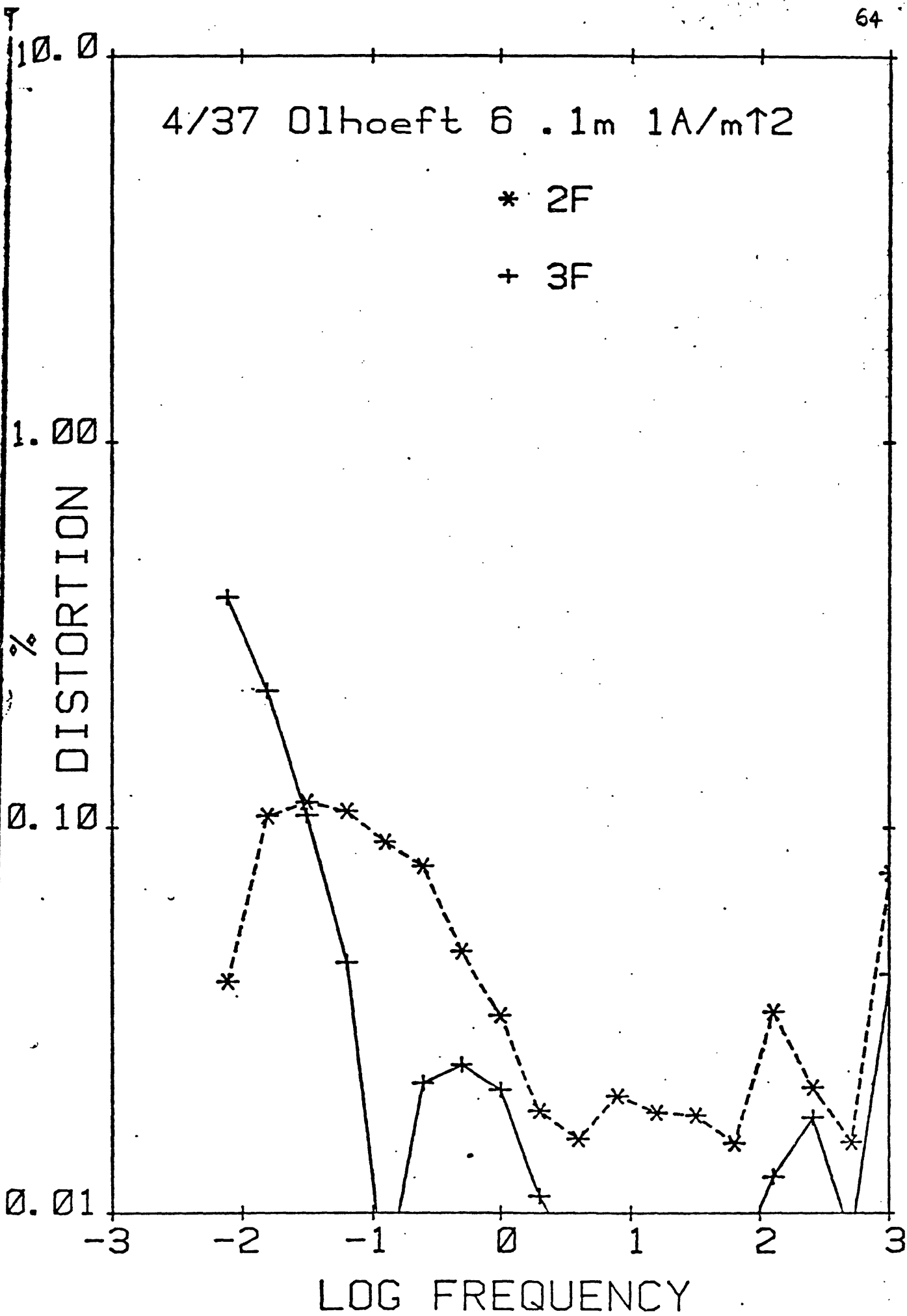
4/37 Olhoeft 6 .1m 1A/m↑2
* 2F
+ 3F
10.0
1.00
0.10
0.01
% DISTORTION
-3
-2
-1
0
1
2
3
LOG FREQUENCY

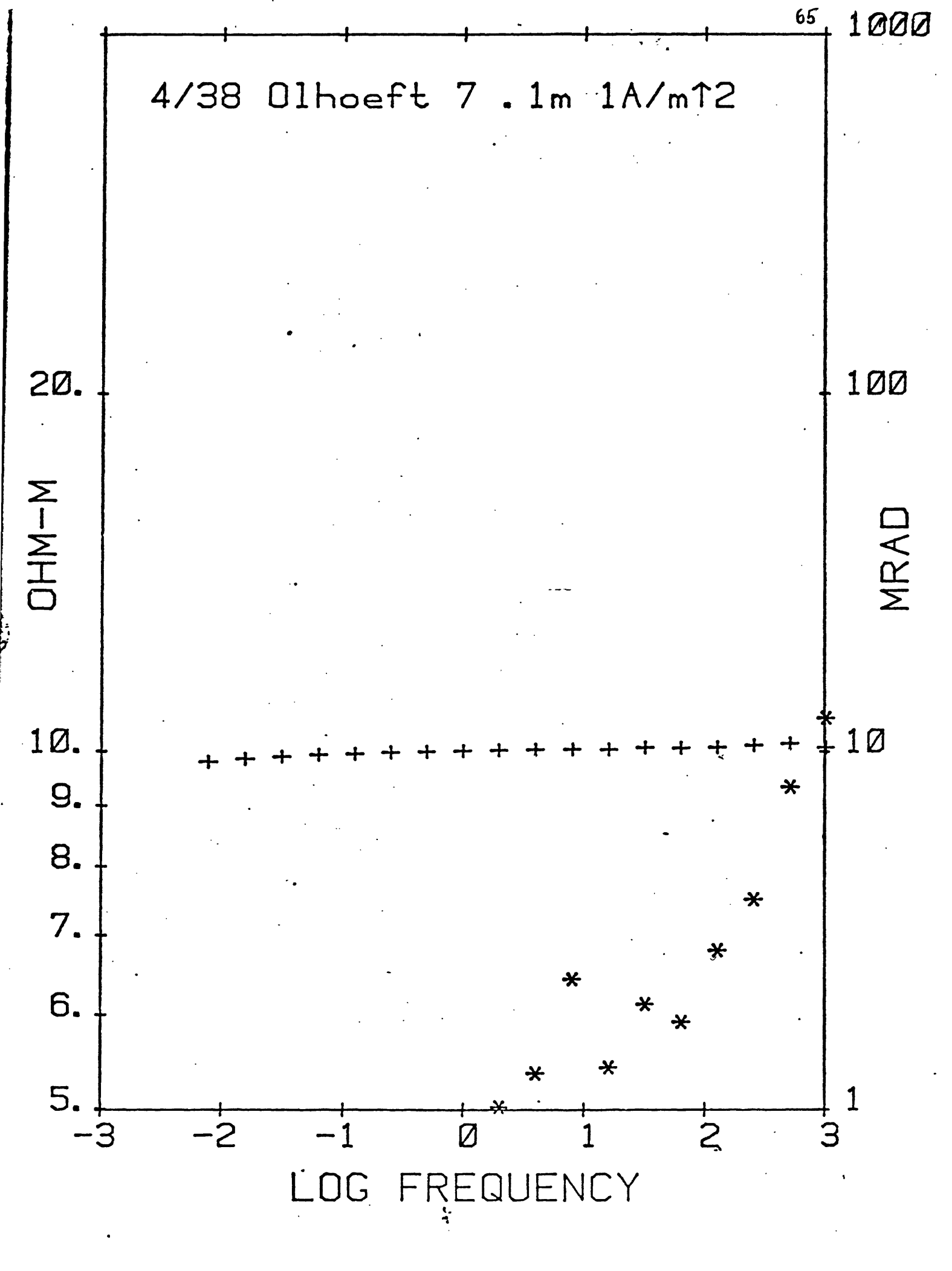
4/38 Olhoeft 7 .1m 1A/m↑2
1000
100
10
1
20.
10.
9.
8.
7.
6.
5.
OHM-M
MRAD
-3
-2
-1
0
1
2
3
LOG FREQUENCY

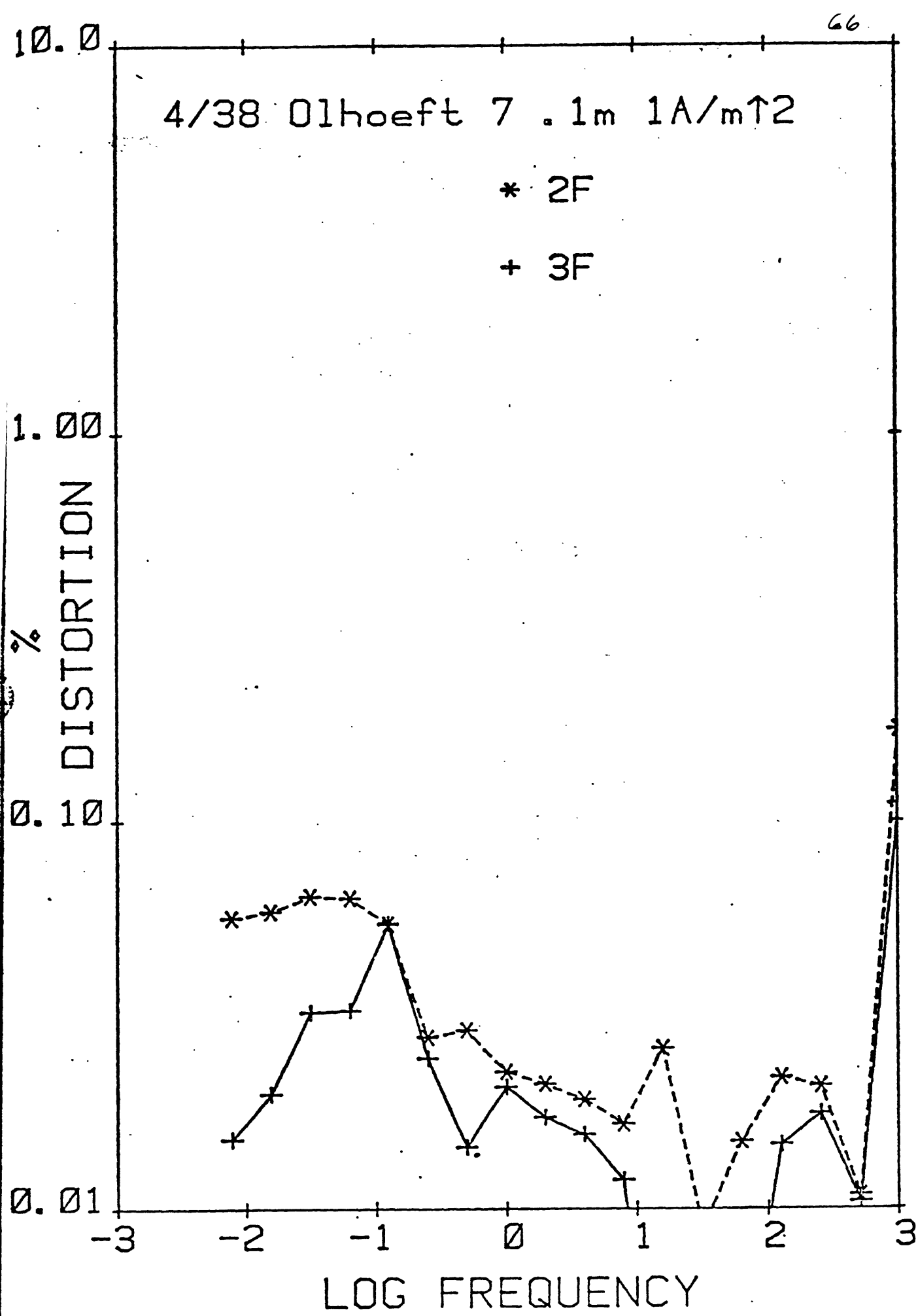
4/38 Olhoeft 7 .1m 1A/m↑2
* 2F
+ 3F
10.0
1.00
0.10
0.01
% DISTORTION
-3
-2
-1
0
1
2
3
LOG FREQUENCY

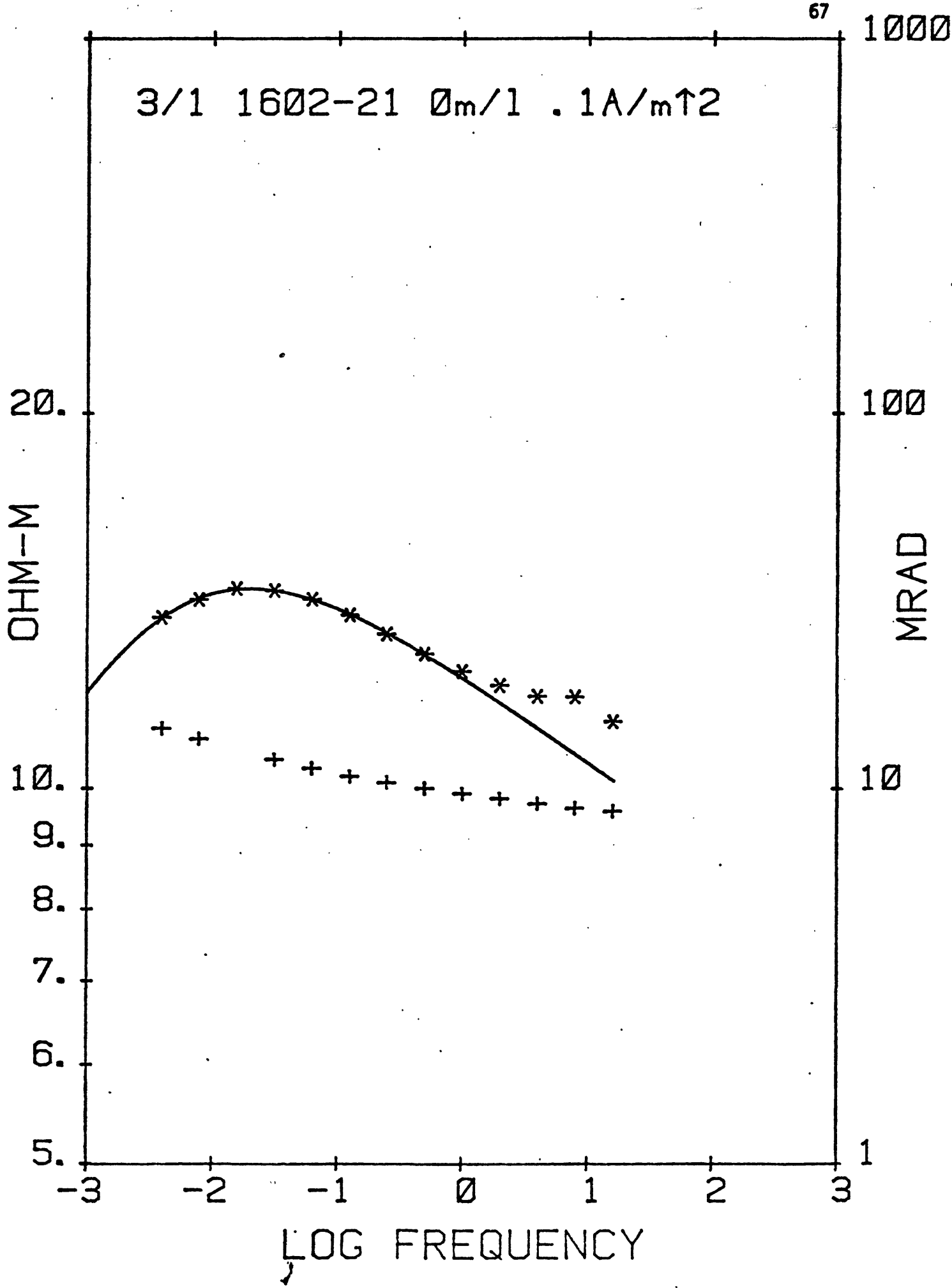
3/1 1602-21 0m/1 .1A/m↑2
1000
20.
100
OHM-M
MRAD
10.
10
9.
8.
7.
6.
5.
1
-3
-2
-1
0
1
2
3
LOG FREQUENCY

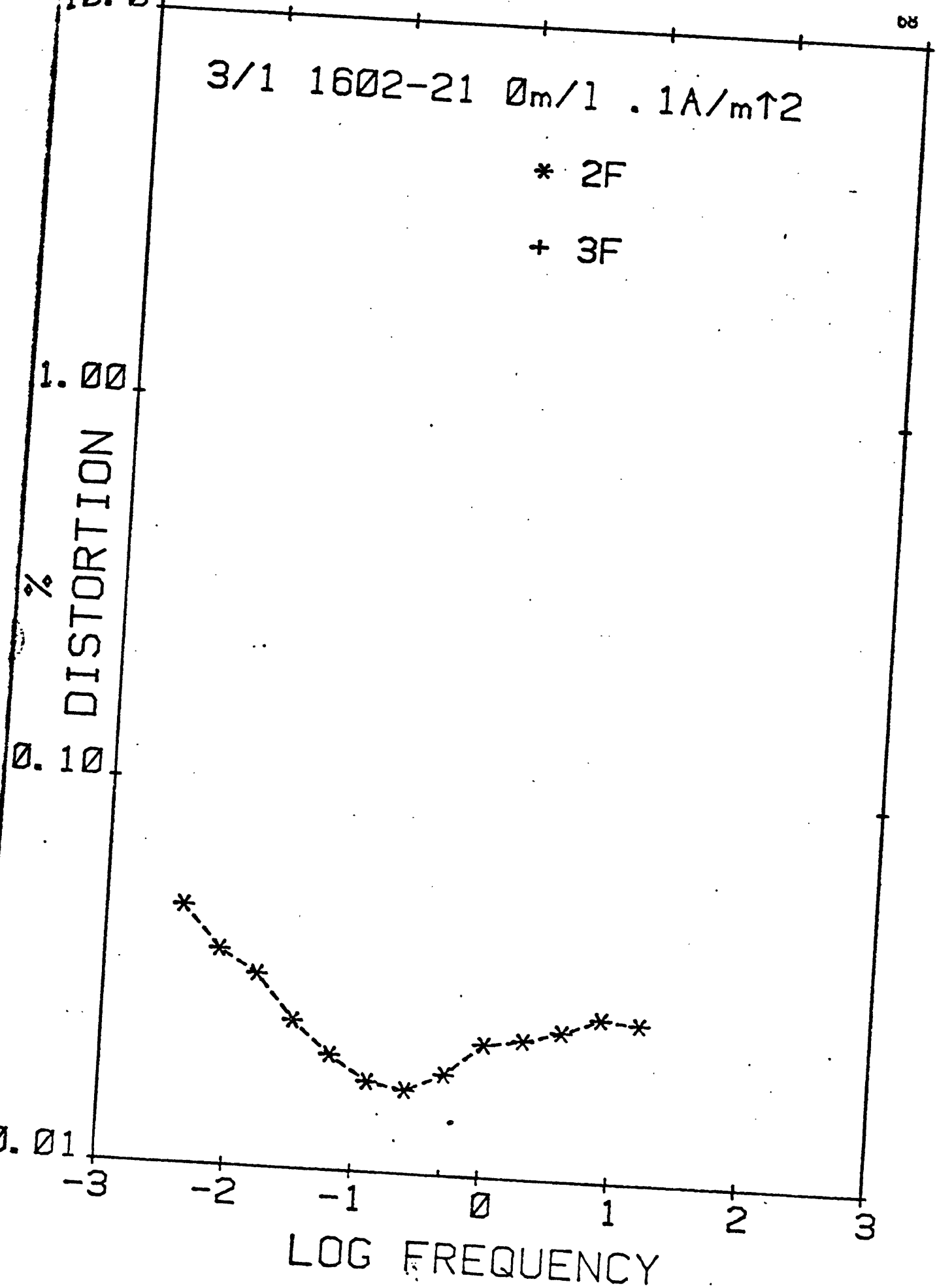
3/1 1602-21 0m/1 .1A/m↑2
* 2F
+ 3F
1.00
% DISTORTION
0.10
0.01
-3
-2
-1
0
1
2
3
LOG FREQUENCY

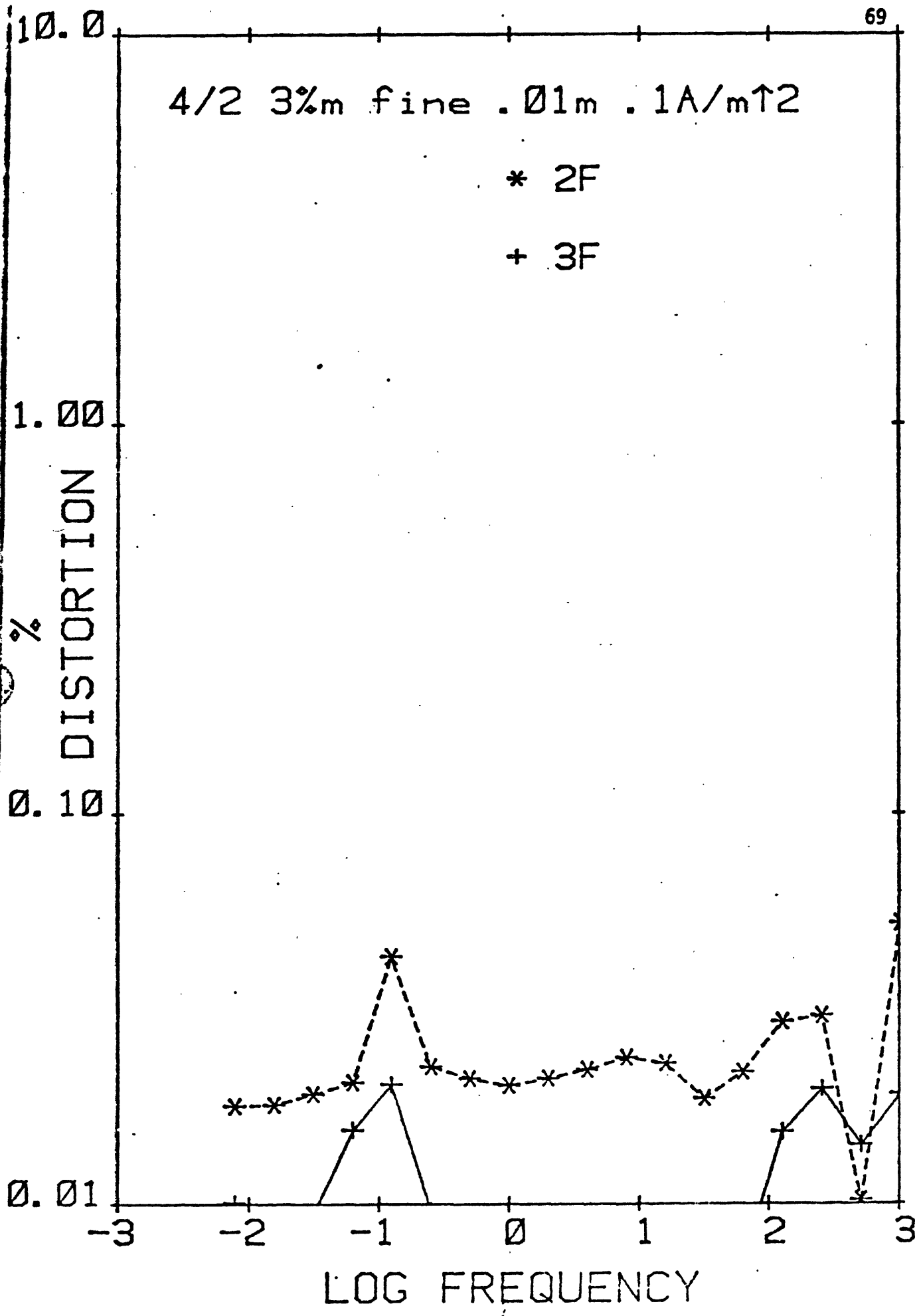
4/2 3%m fine .01m .1A/m↑2
* 2F
+ 3F
10.0
1.00
0.10
0.01
% DISTORTION
-3
-2
-1
0
1
2
3
LOG FREQUENCY

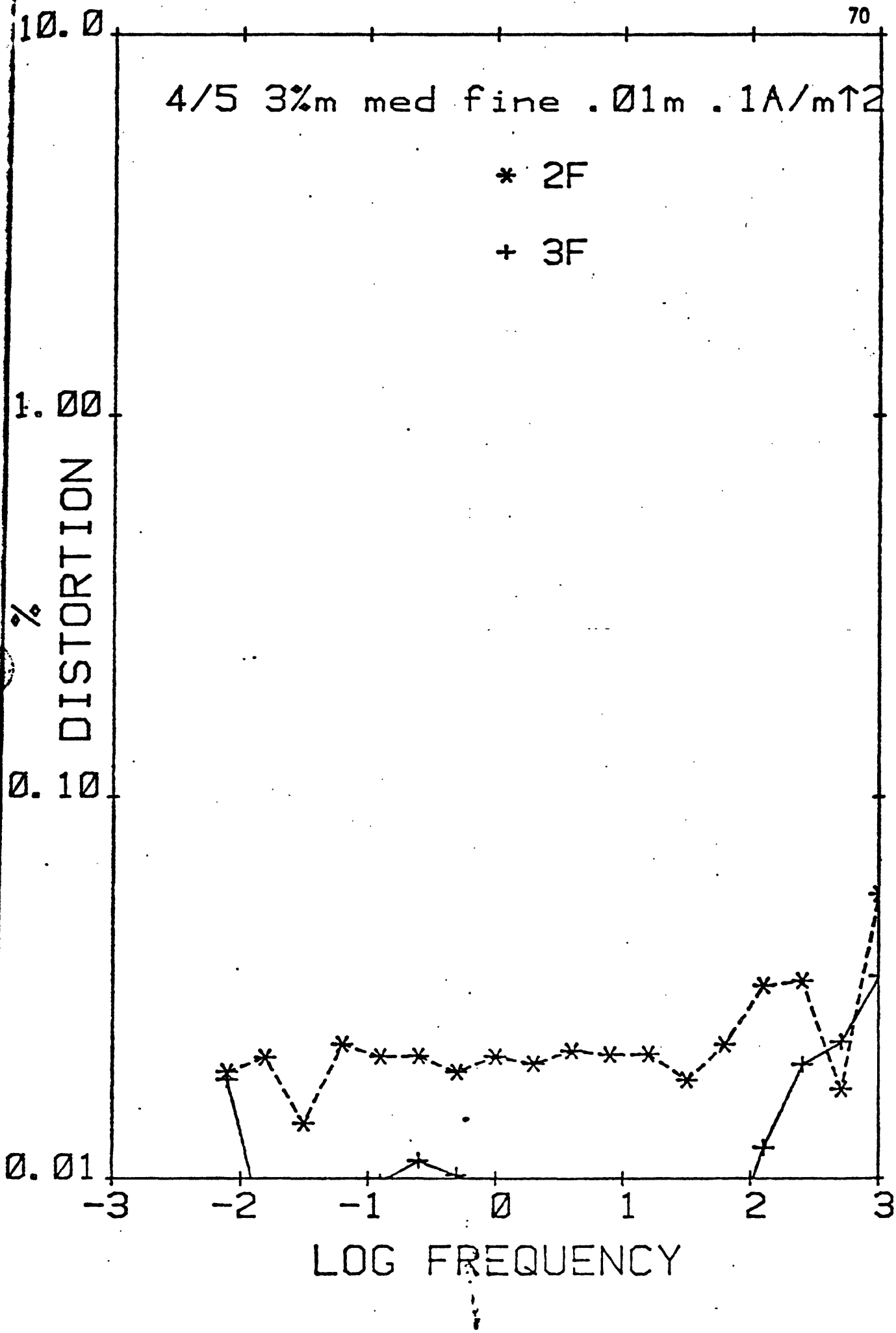
4/5 3%m med fine .01m .1A/m↑2
* 2F
+ 3F
10.0
1.00
0.10
0.01
% DISTORTION
-3
-2
-1
0
1
2
3
LOG FREQUENCY

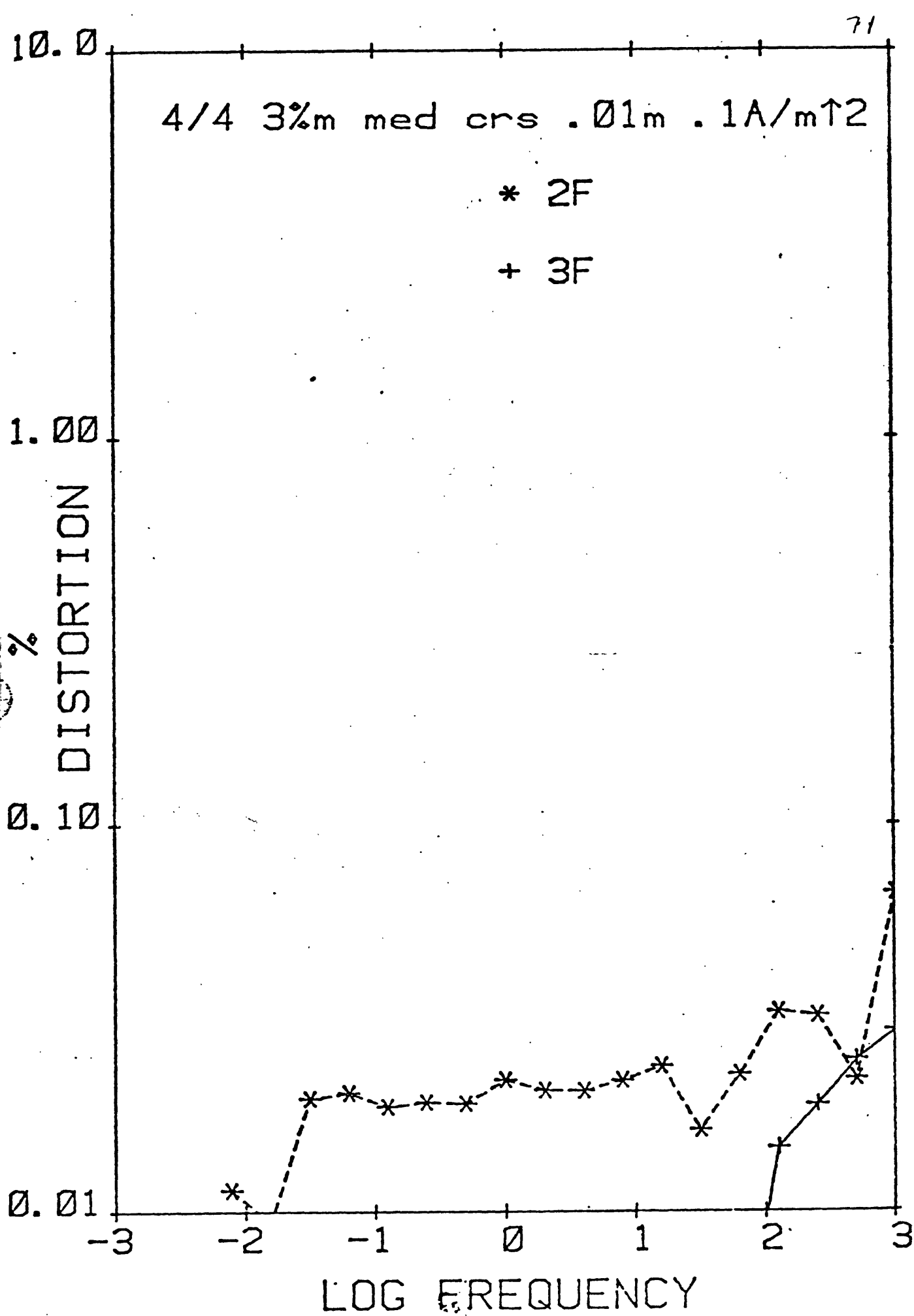
4/4 3%m med crs .01m .1A/m↑2
* 2F
+ 3F
10.0
1.00
0.10
0.01
% DISTORTION
-3
-2
-1
0
1
2
3
LOG FREQUENCY

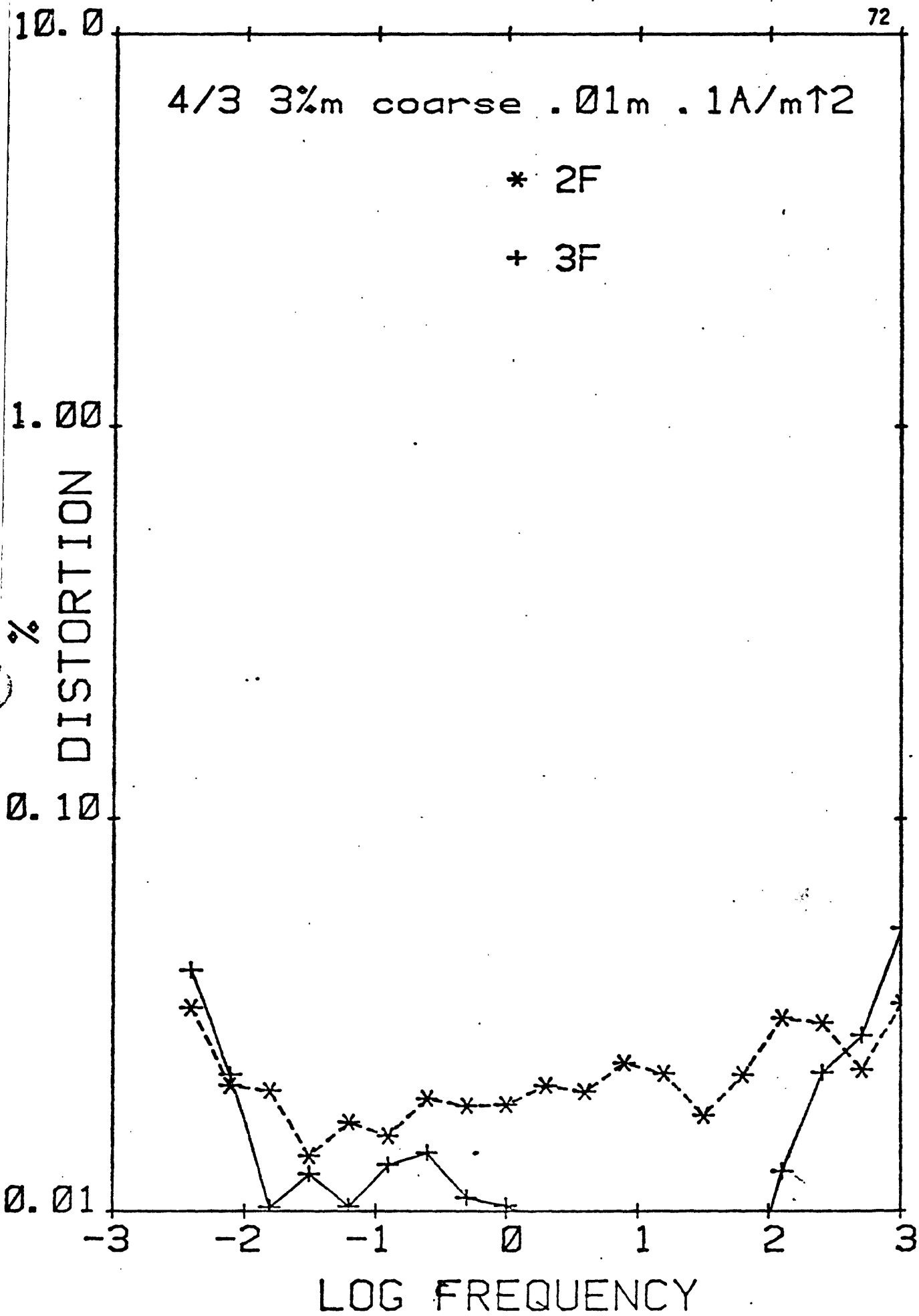
4/3 3%m coarse .01m .1A/m↑2
* 2F
+ 3F
10.0
1.00
0.10
0.01
% DISTORTION
-3
-2
-1
0
1
2
3
LOG FREQUENCY

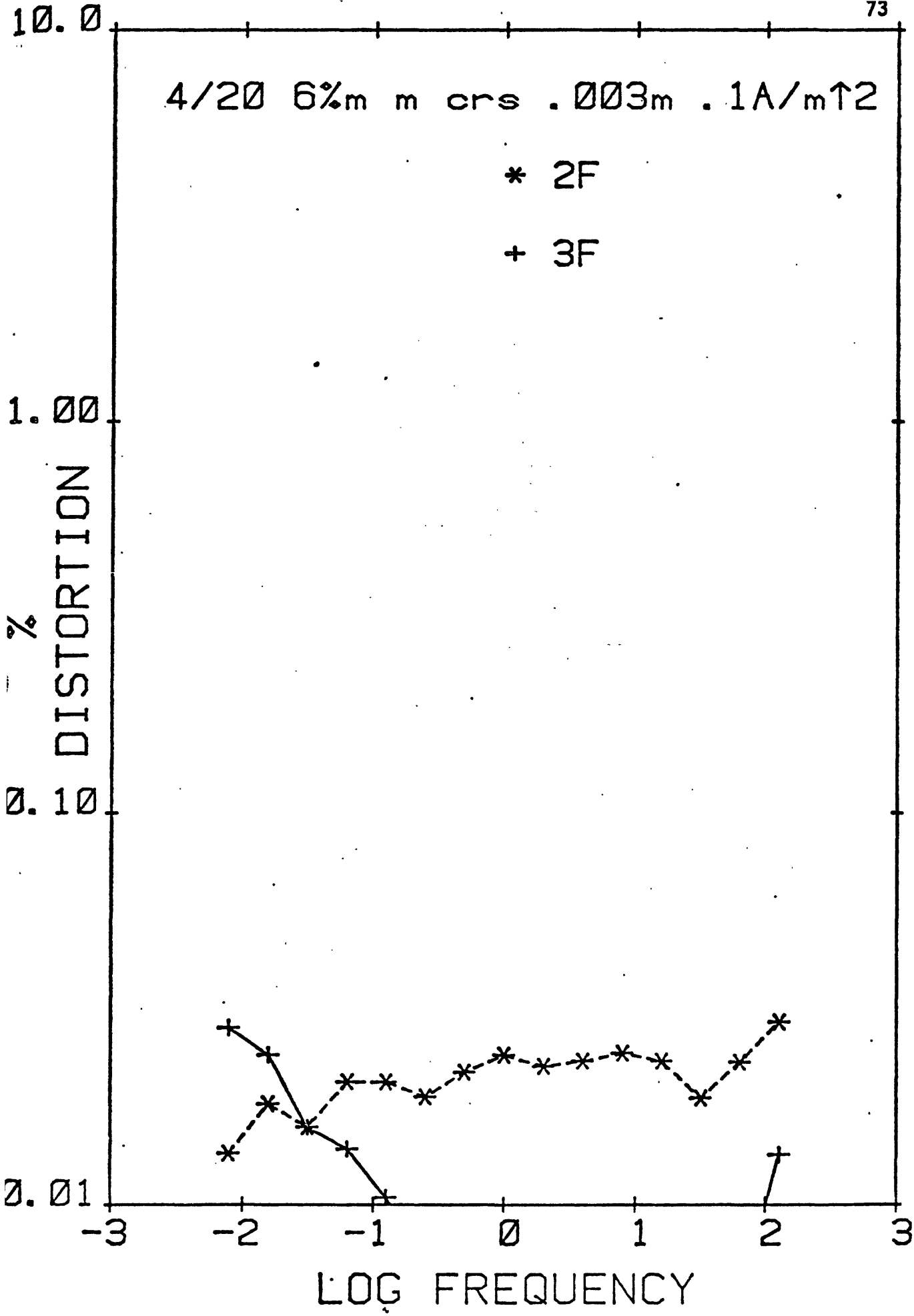
4/20 6%m m crs .003m .1A/m↑2
* 2F
+ 3F
10.0
1.00
0.10
0.01
% DISTORTION
-3
-2
-1
0
1
2
3
LOG FREQUENCY

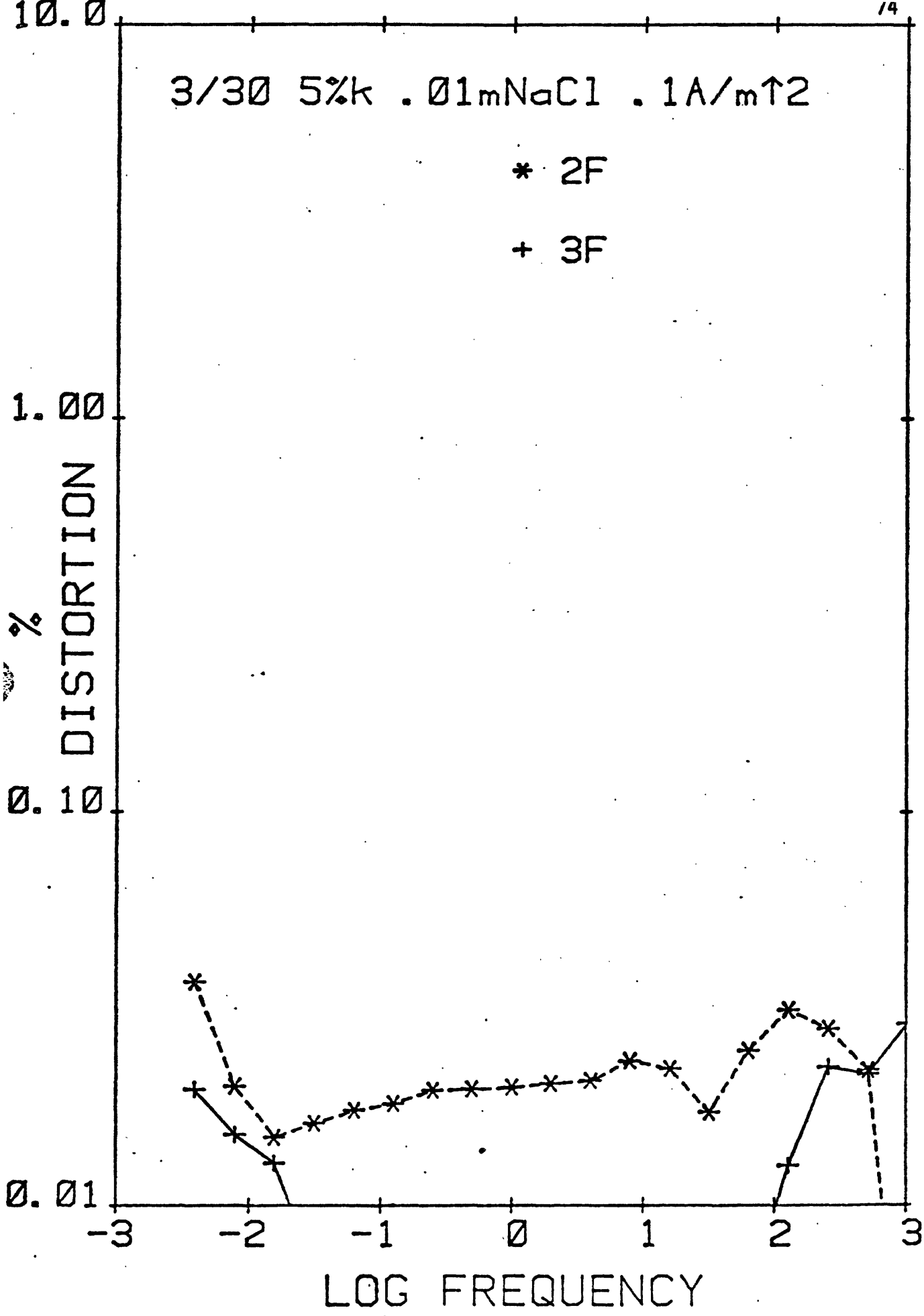
3/30 5%k .01mNaCl .1A/m↑2
* 2F
+ 3F
10.0
1.00
0.10
0.01
% DISTORTION
-3
-2
-1
0
1
2
3
LOG FREQUENCY